Endothelial NOX4-driven oxidative stress inhibition reverses HtrA1 deficiency-induced blood-brain barrier disruption and cognitive impairment

SHI-NA SONG[1,2*], JUN-YING WU[2*], MAO-MEI SONG[1], XIAO-FENG LI[1], JIAN-MING WANG[3], WEN-HUI JIA[4], CHANG-XIN LI[1] and SUI-YI XU[1,5]

[1]Department of Neurology, Headache Center, The First Hospital of Shanxi Medical University, Taiyuan, Shanxi 030001, P.R. China; [2]Department of Rehabilitation, The First Hospital of Shanxi Medical University, Taiyuan, Shanxi 030001, P.R. China; [3]Department of Wound Repair, General Hospital of Taiyuan Iron and Steel Group Co., Ltd., Taiyuan, Shanxi 030003, P.R. China; [4]Department of Neurology, Shanxi Provincial People's Hospital, Taiyuan, Shanxi 030012, P.R. China; [5]Department of Neurology, Headache Center, Shenzhen Baoan People's Hospital, The Second Affiliated Hospital of Shenzhen University, Shenzhen, Guangdong 518000, P.R. China

Received December 8, 2025; Accepted March 26, 2026

DOI: 10.3892/ijmm.2026.5865

Abstract. Heterozygous high temperature requirement serine peptidase A1 (*HTRA1)* mutations are associated with autosomal dominant cerebral small vessel disease (CSVD), but their pathogenic mechanisms remain elusive. In the present study, clinical data were collected from two families carrying heterozygous *HTRA1* mutations, with pathogenic mutations verified through Sanger sequencing. Between January 2018 and December 2023, four patients with CSVD were recruited from the Department of Neurology, First Hospital of Shanxi Medical University (Taiyuan, China). Whole blood RNA sequencing (RNA-seq) was performed to identify differentially expressed genes. Lentiviral vectors were constructed for HtrA1 overexpression and knockdown in mouse brain microvascular endothelial bEnd.3 cells to assess cell viability, oxidative stress, tight junction integrity and apoptosis. Adeno-associated virus (AAV) technology was used to assess how *HtrA1* gene interference affects the function of cerebral vascular endothelial cells in mice. Finally, the NOX4 inhibitor GLX351322 was administered to investigate its regulatory effects on cell permeability and apoptosis. Behavioral changes were assessed through open field and novel object recognition test and Morris water maze experiments to evaluate its impact on cognitive behavior in mice. The present study analyzed clinical data from two enrolled families with heterozygous *HTRA1* mutations [c.854C>T (p.P285L) and c.905G>A (p.R302Q)] and observed stroke, cognitive decline and gait disturbances. RNA-seq of patient blood revealed downregulated *HTRA1*, occludin-like protein 1 and claudin 5, alongside upregulated *NOX4*, with apoptotic pathways prominently enriched. HtrA1 overexpression in bEnd.3 cells enhanced viability, decreased oxidative stress and apoptosis and elevated tight junction protein expression, whereas HtrA1 knockdown exacerbated these effects. In mice, AAV-mediated HtrA1 suppression in cerebrovascular endothelial cells increased NOX4 and caspase3 levels, disrupted blood-brain barrier (BBB) integrity and induced anxiety- and depressive-like behaviors, measured by the open field test, along with cognitive and memory impairment evaluated using the novel object recognition and Morris water maze tests. The NOX4 inhibitor GLX351322 partially restored endothelial function, mitigated BBB damage and alleviated behavioral

Correspondence to: Professor Sui-Yi Xu, Department of Neurology, Headache Center, Shenzhen Baoan People's Hospital, The Second Affiliated Hospital of Shenzhen University, 118 Longjing Er Road, Shenzhen, Guangdong 518000, P.R. China
E-mail: suiyixu@sina.com

Dr Chang-Xin Li, Department of Neurology, Headache Center, The First Hospital of Shanxi Medical University, 85 Jiefangnan Road, Taiyuan, Shanxi 030001, P.R. China
E-mail: lichangxin0351@sina.com

*Contributed equally

Abbreviations: AAV, adeno-associated virus; BBB, blood-brain barrier; CADASIL, cerebral autosomal dominant arteriopathy with subcortical infarcts and leukoencephalopathy; CCK-8, Cell Counting Kit-8; CLDN5, claudin 5; CSVD, cerebral small vessel disease; FLAIR: fluid-attenuated inversion-recovery; GO, Gene Ontology; HC, healthy control; HTRA1mc, high-temperature requirement serine peptidase A1 mutation carrier; KEGG, Kyoto Encyclopedia of Genes and Genomes; MDA, malondialdehyde; MMSE, Mini-Mental State Examination; MoCA, Montreal Cognitive Assessment; MOI, multiplicity of infection; MWM, Morris water maze; NOI, novel object recognition index; NORT, novel object recognition test; NOX4, NADPH oxidase 4; OCEL1, occludin-like protein 1; OFT, open-field test; RT-q, reverse transcription-quantitative; seq, sequencing; ROS, reactive oxygen species; RTCA, real-time cellular analysis; SOD, superoxide dismutase; TGF-β, transforming growth factor-β; WMH, white matter hyperintensity

Key words: heterozygous *HTRA1* mutation, CSVD, oxidative stress, apoptosis, blood-brain barrier

impairment. The present findings demonstrated that heterozygous *HTRA1* mutations promoted CSVD via NOX4-mediated oxidative stress, endothelial dysfunction and BBB breakdown. Targeting the HTRA1-NOX4 interaction using GLX351322 rescued cerebrovascular and cognitive pathology, offering preclinical validation for therapeutic intervention.

Introduction

Cerebral small vessel disease (CSVD) is a complex neurological condition characterized by compromised blood flow and structural abnormalities in the small blood vessels of the brain (1). The clinical manifestations of CSVD include cognitive decline, stroke and severe neurological deficit (2). The underlying mechanisms that trigger CSVD are multifaceted, entailing an intricate interplay among vascular conditions, inflammation and neuronal integrity (3,4). The current treatments (antiplatelet agents, statins and risk factor management) for CSVD often fail to yield satisfactory outcomes, warranting the need for a comprehensive understanding of the pathogenic mechanisms involved to develop effective and safe treatments.

The high-temperature requirement serine peptidase A1 (HTRA1) belongs to the serine protease family, which is involved in proteolysis and cell fate determination (5). It exhibits dual activity as a chaperone and serine protease (6). HTRA1 plays crucial roles in physiological processes, including extracellular matrix remodeling by hydrolyzing fibronectin, decorin, aggrecan and elastin (7-9) and regulating growth factors such as transforming growth factor-β (TGF-β) (10,11). The expression levels of HTRA1 vary across tissues and under various conditions, notably in blood vessels (12,13), which are involved in numerous physiological processes. Recently, HTRA1 has been implicated in age-associated macular degeneration, osteoarthritis, cancer, and CSVD (14,15). Several heterozygous and homozygous *HTRA1* mutations cause CSVD (16,17). Heterozygous *HTRA1* mutations cause cerebral autosomal dominant arteriopathy with subcortical infarcts and leukoencephalopathy (CADASIL) type 2, also known as heterozygous *HTRA1* mutation carrier (mc) (18). Previous research has primarily focused on case reports and potential pathogenic mechanisms associated with mutation sites (19,20). Partial site mutations in *HTRA1* can lead to the downregulation of *HTRA1* mRNA and protein expression, resulting in reduced HTRA1 protease activity (21-23). Decreased HTRA1 protease activity is the primary pathogenic mechanism underlying HTRA1-associated CSVD. However, the endothelial-specific mechanisms linking *HTRA1* mutations to CSVD phenotypes remain elusive and the functional consequences of partial HTRA1 deficiency on cerebrovascular homeostasis are underexplored (17).

Materials and methods

Subjects. Between January 2018 and December 2023, four patients (three male, one female; age range, 44-54 years; median age, 47.5 years) diagnosed as heterozygous *HTRA1*mcs and four healthy controls (HCs; three male, one female; age range, 43-53 years; median age, 48 years) were recruited from the Department of Neurology, First Hospital of Shanxi Medical University (Taiyuan, China). The inclusion criteria were as follows: i) confirmation of a heterozygous *HTRA1* mutation by genetic testing; ii) presence of typical CSVD-related neuroimaging features on brain MRI; iii) age between 18 and 60 years; and iv) provision of written informed consent. The exclusion criteria were as follows: i) other hereditary or acquired causes of CSVD; ii) presence of severe systemic diseases; iii) history of stroke not attributable to CSVD; and iv) any contraindication to MRI. Inclusion criteria for HCs were: i) absence of *HTRA1* mutations confirmed by genetic screening; ii) no clinical symptoms or neuroimaging features suggestive of CSVD; iii) age and sex matched to the patient group; and iv) provision of written informed consent. Exclusion criteria for HCs were: i) any history of neurological disorders; ii) significant systemic illnesses; or iii) any contraindications to MRI; iv) any abnormal findings on brain MRI suggestive of CSVD or other intracranial pathologies.

All patients exhibited typical CSVD imaging features, with brain magnetic resonance imaging (MRI) lesions corresponding to the clinical symptoms. The brain MRI scans were performed using a 3.0-Tesla Siemens MAGNETOM Prisma scanner. T2-weighted fluid-attenuated inversion recovery (FLAIR) sequences were acquired with the following parameters: Repetition time, 9,000 msec, echo time, 94 msec, and inversion time, 2,500 msec. Clinical and imaging data were assessed from the probands and their family members. Cognitive function was evaluated using the Montreal Cognitive Assessment (MoCA) and the Mini-Mental State Examination (MMSE). The study was approved by the ethics committee of the First Hospital of Shanxi Medical University (approval no. KYLL-2024-161), and all participants provided written informed consent. Peripheral blood samples were collected from patients for genetic analysis and HCs.

Sanger sequencing. Genomic DNA was analyzed via Sanger sequencing of DNA extracted from peripheral blood collected from the probands, family members and HCs in anticoagulant EDTA-coated tubes. Genomic DNA was extracted using the Ezup Column Blood Genomic DNA Extraction kit (Sangon Biotech, cat. no. B518253) according to the manufacturer's instructions. PCR was performed using Taq Plus DNA Polymerase (Sangon Biotech, cat. no B600090). Thermocycling conditions were as follows: Initial denaturation at 95˚C for 5 min; followed by 40 cycles of denaturation at 95˚C for 30 sec, annealing at 58˚C for 30 sec, and elongation at 72˚C for 30 sec; with a final extension at 72˚C for 10 min. The PCR products were detected by 1% agarose gel electrophoresis. Following purification by gel extraction, the products were sequenced on a 3730XL sequencer (Applied Biosystems). Sanger sequencing and primer synthesis (Table I) were performed by Sangon Biotech Co., Ltd. The pathogenicity of the HTRA1 heterozygous mutations c.854C>T (p.P285L) and c.905G>A (p.R302Q) was assessed using bioinformatics tools, including Polyphen-2 (http://genetics.bwh.harvard.edu/pph2), Sorting Intolerant From Tolerant (/sift.bii.a-star.edu.sg), Mutation Taster (https://www.mutationtaster.org), Combined Annotation Dependent Depletion (https://cadd.gs.washington.edu/score), non-synonymous single nucleotide polymorphism (nsSNP) Analyzer (https://snpanalyzer.uthsc.edu) and Mutation Assessor (http://mutationassessor.org/r3). According to the Ensembl database (https://www.ensembl.org), both mutations

Table I. Primer sequences.

Primer	Sequence, 5'→3'	Product size, bp
HTRA1 c.854 C>T	Forward: TTGGTTTTCCATGATATCTGTGC Reverse: GTTGATGATGGCGTCGGTCT	275
HTRA1 c.905 G>A	Forward: GTGGTCGCCATCGGAAGC Reverse: ATCACCCTAAAGCACCCAATAC	384

HTRA1, high temperature requirement serine peptidase A1.

were identified as single nucleotide polymorphisms, specifically c.854C>T (rs587776446) and c.905G>A (rs2133449474). The aforementioned tools predicted that both mutations were deleterious and likely pathogenic, indicating a notable impact on HTRA1 function and potential involvement in associated phenotypic mechanisms.

RNA-seq. Total RNA was extracted using TRNzol Universal Reagent (cat. no. DP424; TIANGEN Biotech Co., Ltd.) according to the manufacturer's instructions. RNA integrity was assessed using the Agilent 5400 Fragment Analyzer System (Agilent Technologies), and the RNA integrity number (RIN) was determined for each sample. Sequencing libraries were prepared and subjected to paired-end (PE) sequencing with a read length of 150 bp (2x150 bp) on the Illumina NovaSeq X Plus platform (Illumina, Inc.) using the NovaSeq X Series 25B Reagent Kit (300 cycles; cat. no. 20104706; Illumina, Inc.). The final library loading concentration was measured by quantitative PCR (qPCR) and was 4.03 nM for patient samples and 4.24 nM for normal controls. RNA-seq was performed by Novogene Co., Ltd. Raw reads were filtered to remove adapters and low-quality sequences, aligned to the human genome (GRCh38: obtained from the NCBI, assembly accession: GCF_000001405.26) using HISAT2 (daehwankimlab.github.io/hisat2/), and quantified using feature counts. Differential expression analysis [DESeq2 (https://pubmed.ncbi.nlm.nih.gov/25516281), $|\log_2 FC|>1$, FDR-adjusted P<0.05] was used to identify significant genes, which were visualized using volcano or heatmaps. Principal Component Analysis (PCA) was performed on the normalized expression data of all detected genes using the prcomp function in R software (version 4.3.1). Gene Ontology (GO, http://geneontology.org/) and Kyoto Encyclopedia of Genes and Genomes (KEGG; kegg.jp/) pathway enrichment analyses were conducted using cluster Profiler (FDR <0.05) (version 4.19.6; https://doi.org/10.1089/omi.2011.0118).

ELISA. Anticoagulant-coated blood collection tubes were used to collect 3-5 ml venous blood from the HTRA1mc and HC groups. Following standing at 25˚C for 30 min, the blood was centrifuged at 1,200 x g for 10 min at 4˚C to obtain plasma, divided into microcentrifuge tubes, and centrifuged at 3,200 x g for another 10 min at 4˚C to remove platelets. The expression levels of HTRA1 (cat. no. HM11176) and NADPH oxidase 4 (NOX4; both Bioswamp Life Science Lab; Wuhan Bienle Biotechnology Co., Ltd.; cat. no. HM11179) were measured using ELISA kits, in accordance with the manufacturer's instructions.

Construction of HtrA1 overexpression (OE) and knockdown lentiviral vectors. The lentiviral vectors for OE included mCherry red fluorescent LV8N (EF-1a/mCherry&Puro) and non-fluorescent LV6 (EF-1a/Puro) shuttle plasmid vectors. For knockdown, the short hairpin (sh)HtrA1-RNA lentiviral vectors included GFP green fluorescent LV3 (H1/GFP&Puro) and non-fluorescent LV2 (U6/Puro) shuttle plasmid vectors (GenePharma). The coding and protein sequences of mouse *HtrA1* were obtained from the National Center for Biotechnology Information (NCBI) (https://www.ncbi.nlm.nih.gov/). The *HtrA1* gene fragments were cloned into the *Not*I/*Nsi*I sites of the LV8N and LV6 shuttle plasmid vectors. Following verification via Sanger sequencing, the *HtrA1* gene OE plasmid was constructed. The following shRNA sequences were incorporated into the LV3 and LV2 shuttle plasmids for the mouse *HtrA1* gene: shRNA-HtrA1-mus-749, 5'-GGGTCAAGGTTGAGCTGAAGA-3'; shRNA-HtrA1-mus-885, 5'-GCTGAGACCTGGAGAATTTGT-3'; shRNA-HtrA1-mus-1079, 5'-GCGAGGTGATTGGGATTAACA-3'; and negative control (NC), 5'-TTCTCCGAACGTGTCACGT-3'.

Recombinant viral plasmids for HtrA1 OE and knockdown, along with three auxiliary packaging plasmids (PG-P1-VSVG, PG-P2-REV and PG-P3-RRE) (GenePharma), were subjected to high-purity non-toxic endotoxin extraction. Plasmid DNA was extracted using a high-purity midi-prep kit (Shanghai GenePharma Co.) and dissolved in sterile double-distilled water. The concentration and purity of plasmid DNA were determined by UV spectrophotometry, and only samples with an A260/A280 ratio between 1.8 and 2.0 were used for subsequent experiments. For lentivirus production, the third-generation lentiviral packaging system was used. 293T cells (GenePharma) were co-transfected with RNAi-Mate reagent (GenePharma, cat. no. G04001) at 37˚C. In total, 20 μg plasmid DNA was used, composed of the recombinant HtrA1-OE or HtrA1-shRNA plasmid and three helper plasmids (PG-P1-VSVG, PG-P2-REV, PG-P3-RRE) at a 1 : 1 : 1 : 1 mass ratio (2.5 μg each). After 48 h, the lentiviral supernatant was collected, filtered (0.45 μm), and concentrated. The final lentivirus titer was determined to be $\geq 1x10^8$ TU/ml (GenePharma). bEnd.3 cells were infected at an MOI of 125 (Table II). The virus-containing medium was removed after 24 h and replaced with fresh medium. Following a 48-h recovery, transduced cells were selected and maintained in medium containing 5 μg/ml puromycin.

Culture and viral infection of bEnd.3 cells. The bEnd.3 cells (Procell Life Science) were cultured in high-glucose DMEM

Table II. Lentivirus vector titers.

Lentiviral vector	Titer, TU/ml
LV8N-NC	$2.00x10^8$
LV8N-HtrA1	$3.00x10^8$
LV3-NC	$5.00x10^8$
LV3-HtrA1-Mus-749	$1.00x10^8$
LV3- HtrA1-Mus-885	$1.00x10^8$
LV3- HtrA1-Mus-1079	$1.00x10^8$
LV6-NC	$1.29x10^8$
LV6-HtrA1	$2.05x10^8$
LV2-NC	$4.00x10^8$
LV2- HtrA1-Mus-1079	$1.85x10^8$

NC, negative control; HtrA1, high temperature requirement serine peptidase A1.

(HyClone; Cytiva; cat. no. SH30022.01) supplemented with 10% FBS (Wuhan Boster Biological Technology, Ltd.; cat. no. PYG0001) at 37˚C in a 5% CO_2 atmosphere. Upon reaching ~50% confluence, the cells were exposed to serum-free high-glucose DMEM along with lentiviral supernatant over-expressing HtrA1 [multiplicity of infection=125]. After 24 h incubation, the medium was replaced with complete medium containing 10% FBS. After 72 h, 5 μg/ml puromycin was used for screening of HtrA1 OE and knockdown cells for 96 h. The groups were as follows: Untransfected (UT)-OE; NC-OE (bEnd.3 cells infected with LV8N-NC or LV6-NC lentiviral supernatant); HtrA1-OE (bEnd.3 cells infected with LV8N-HtrA1 or LV6-HtrA1 lentiviral supernatant); sh-UT; sh-NC (bEnd.3 cells infected with LV3-NC or LV2-NC lentiviral supernatant); and sh-HtrA1 (bEnd.3 cells infected with LV3 or LV2 lentiviral supernatant). Cells in the sh-HtrA1 group were treated with 5 μM GLX351322 (MedChemExpress; cat. no. HY-100111) for 24 h at 37˚C to downregulate the expression of NOX4.

Reverse transcription-quantitative (RT-q) PCR. Total RNA was extracted from cells using TRIzol reagent (Invitrogen, cat. no. 15596-026), followed by chloroform and isopropanol precipitation. RNA concentration and purity were assessed using a Take3 micro-detection plate (BioTek, RNA samples were reverse transcribed into cDNA using the PrimeScript RT reagent kit with gDNA Eraser according to the manufacturer's protocol (Takara Bio, Inc.; cat. no. RR047A). The obtained cDNA was amplified using a Roche Diagnostics LightCycler480II. The 20 μl reaction mixture comprised 10.0 μl TB Green Premix Ex TaqII (Takara Bio, Inc.; cat. no. RR820A), 2.0 μl cDNA, 6.4 μl diethylpyrocarbonate water and 0.8 μl (10 μM) primer. Thermocycling conditions were as follows: Initial denaturation at 95˚C for 30 sec, followed by 40 cycles of denaturation at 95˚C for 5 sec, and annealing/extension at 60˚C for 30 sec. GAPDH was used as an endogenous reference for the normalization of mRNA expression. The *HtrA1* mRNA levels were determined using the $2^{-\Delta\Delta Cq}$ method (24). The primer sequences (Sangon Biotech Co., Ltd.) were as follows: HtrA1 forward, 5'-tgacg-gcgggcatctccttc-3' and reverse, 5'-tcttggtgacagctttccctttgg-3' and GAPDH forward, 5'-ccctggccaaggtcatccat-3' and reverse, 5'-tcacgccacagctttccaga-3'.

Western blotting. bEnd.3 cells and mouse brain tissue samples were lysed in RIPA lysis buffer (cat. no. AR0102-100) containing broad-spectrum protease inhibitors (both Wuhan Boster Biological Technology Co.; cat. no. AR1182). Protein concentration was determined using a BCA protein assay kit (Wuhan Boster Biological Technology Co.; cat. no. AR0146) following the manufacturer's instructions. Equal amounts (30 μg) of protein were separated by 10% SDS-PAGE, followed by transfer onto a 0.22 μM polyvinylidene fluoride membrane. The membranes were blocked at room temperature for 2 h with 5% (w/v) non-fat dry milk in 0.1% TBST. After blocking for 2 h, the membranes were incubated overnight with primary antibodies at 4˚C as follows: Rabbit anti-HtrA1 (1:250, Wuhan Boster Biological Technology Co.; cat. no. A01801-1), anti-occludin (cat. no. A2601), anti-zona occludens (ZO)1 (both 1:1,000, both ABclonal Biotech Co., Ltd.; A0659), anti-claudin (CLDN)5 (1:250, BIOSS; cat. no. bs-10296R), anti-NOX4 (Wuhan Boster Biological Technology Co.; cat. no. BM4135), anti-caspase3 (both 1:1,000, ABclonal Biotech Co., Ltd.; cat. no. A2156), anti-GAPDH (1:5,000, Shanghai Abways Biotechnology Co., Ltd.; cat. no. AB0037) and anti-β-actin (1:5,000, ABclonal Biotech Co., Ltd.; cat. no. AC038). After washing the membrane with TBST, it was incubated with goat anti-rabbit IgG-HRP secondary antibody (1:5,000; Wuhan Boster Biological Technology Co., Ltd.; cat. no. BA1054) for 90 min at 25˚C. The luminescent solution was prepared using the ECL Luminescent Substrate kit (Wuhan Boster Biological Technology Co., Ltd.; cat. no. AR1171) and the bands were visualized using an imaging analysis system (Bio-Rad Laboratories, Inc.; Chemidoc MP). The gray value of the target proteins was analyzed using the ImageJ software (V1.8.0; National Institutes of Health).

Cell Counting Kit-8 (CCK-8) assay. A total of $5x10^3$ cells was seeded in a 96-well plate. After 12, 24, 48 and 72 h, cells were treated with working solution containing 10 μl CCK-8 solution (MedChemExpress; cat. no. HY-K0301) and 90 μl DMEM with 10% FBS. After 2 h incubation in the dark, the absorbance was measured at 450 nm using a multifunctional microplate reader (BioTek; Agilent Technologies, Inc.; Synergy H1).

Real-time cellular analysis (RTCA). RTCA was performed using the RTCA S16 system (ACEA Biosciences, Inc.). A total of 50 μl DMEM with 10% FBS in E-plate16 wells was used for determining the baseline. bEnd.3 cells were seeded at a density of $5x10^3$ cells/well in the wells of E-plate16. Following 30 min incubation at 37˚C, RTCA was performed for 72 h, with impedance measured at 15-min intervals.

Immunofluorescence staining of cells. A total of $5x10^3$ bEnd.3 cells was seeded in 24-well plates. The cells were fixed with 4% paraformaldehyde at room temperature for 30 min. Following washing with PBS, 0.5% Triton X-100 (Beyotime Biotechnology; cat. no. P0096-500 ml) was added at room temperature for permeabilization of cell membrane. Blocking was performed using 5% BSA (Bossis; cat. no. AR1006) for 2 h at 25˚C. The cells were then incubated overnight at 4˚C with

the primary antibodies as follows: Rabbit anti-CLDN5 (1:100, ABclonal Biotech Co., Ltd.; A10207), anti-occludin (1:150, Bossis; cat. no. bs-10011R), anti-ZO1 (1:150, ABclonal Biotech Co., Ltd.; cat. no. A0659) and anti-NOX4 (1:100, Wuhan Boster Biological Technology Co. Ltd.; BM4135). Cells were washed three times with PBS with 0.1% Tween-20 (PBST) and incubated with Alexa Fluor 555-labeled donkey (1:500, cat. no. A0453) and Alexa Fluor 488-labeled goat anti-rabbit IgG (H+L; 1:200, both Beyotime Biotechnology; cat. no. A0423) at 25˚C for in the dark for 2 h. The cells were washed three times with PBST for 15 min and imaged under a confocal microscope (Leica GmbH). Fluorescence intensity was analyzed using ImageJ software (V1.8.0; National Institutes of Health).

FITC-dextran permeability assay. A total of $2x10^5$ cells were seeded in the upper chamber of a 24-Transwell system (8 μm, Falcon; Corning Life Sciences; cat. no. 353097) and incubated at 37˚C in a humidified 5% CO_2 incubator for 24 h. The upper chamber was filled with 200 μl DMEM (HyClone; Cytiva) with 10% FBS (Boster, cat. no. PYG0001), whereas the lower chamber contained 600 μl PBS. Following 12 h incubation at 37˚C, the medium from the upper chamber was removed and the cells were washed three times with PBS. A total of 100 μl 1 μg/ml FITC-dextran (40,000 MW, Sigma-Aldrich; Merck KGaA; cat. no. SLCB8958) was added to the upper chamber. The medium in the lower chamber was discarded and replaced with 600 μl PBS. After the 1 h incubation at 37˚C, the fluorescence intensity was measured using the SpectraMax i3x detection system at excitation/emission (Ex/Em) wavelengths of 485/528 nm (Molecular Devices, LLC).

Reactive oxygen species (ROS) assay. bEnd.3 cells ($1.5x10^5$) were seeded in a 6-well plate and cultured for 24 h at 37˚C. DCFH-DA (MedChemExpress; cat. no. HY-D0940) staining was performed when the cell density reached 80%. The culture medium was discarded and the cells were washed three times with PBS. Subsequently, the cells were incubated with 1 ml DCFH-DA working solution at a concentration of 10 μM for 20 min at 37˚C in the dark. Images were captured under a fluorescence microscope (Ex/Em=488/525 nm) and the fluorescence intensity was analyzed using ImageJ software (V1.8.0, National Institutes of Health).

Superoxide dismutase (SOD) and malondialdehyde (MDA) assay. The cells were detached using 0.25% trypsin (Beijing Solarbio Science & Technology Co., Ltd.; cat. no. T1300). The cells were lysed using RIPA lysis buffer (Beijing Solarbio, cat. no. R0010) containing 50 mM Tris (pH 7.4), 150 mM NaCl, 1% Triton X-100, 1% sodium deoxycholate, and 0.1% SDS. The protein concentration was measured using the BCA method. The activity of SOD and MDA were determined using the SOD (cat. no. A001-3) and MDA Detection kits (both Nanjing Jiancheng Bioengineering Institute; cat. no. A003-1-2), according to the manufacturer's instructions.

Apoptosis detection. Apoptosis (early + late apoptotic cells) was detected via flow cytometry using the Annexin V-FITC/propidium iodide (PI) staining kit (Dalian Meilun Biology Technology Co., Ltd.; cat. no. MA0220) following the manufacturer's instructions. Briefly, $2x10^5$ bEnd.3 cells were seeded in 6-well plates and cultured for 24 h at 37˚C. Cells were detached using 0.25% trypsin (Wuhan Boster Biological Technology Ltd.; cat. no. PYG0065) and incubated with 5 μl Annexin V-FITC/PI staining solution for 15 min at 25˚C in the dark. Flow cytometry was performed using a NovoCyte 3130 instrument (ACEA Biosciences, Inc.). Red and green fluorescence signals were recorded and analyzed using the NovoExpress software (Version 1.5.0, ACEA Biosciences, Inc.).

AAV/B130-shHtrA1 mouse model. All animal experiments were approved by the Animal Welfare and Ethics Committee of the First Hospital of Shanxi Medical University (approval no. DWYJ-2025-304, Taiyuan, China). Male C57BL/6J mice (Spef Biotechnology Co., Ltd.; age, 6-8 weeks) were housed in a specific pathogen-free animal facility at 25±2˚C, 50-60% relative humidity and a 12/12-h light/dark cycle with free access to food and water (n=24, weight, 20-25 g). Humane endpoints were as follows: i) loss of more than 20 % of initial body weight within 24 h, ii) inability to reach food or water, iii) persistent hunched posture with ruffled fur, iv) moribund state and v) respiratory distress. Animals reaching any of these endpoints were immediately euthanized by cervical dislocation. None of the animals reached the predefined humane endpoints during the study. The endothelial cell-specific HtrA1-shRNA mouse model was created by injecting AAV HBAAV2/BI30-m-HtrA1-shRNA-EGFP (Hanbio Biotechnology Co., Ltd., cat. no. 80062053) into the tail vein of C57BL/6J mice. Mice were divided into three groups (n=8): Vehicle (mice injected with saline), AAV/B130-NC (mice injected with a virus control) and AAV/B130-shHtrA1 group (mice injected with HtrA1-interfering AAV). Anesthesia was induced with 5% isoflurane using a compact small animal anesthesia machine (RWD Life Science Co., Ltd.), followed by maintenance with 1.5-2.5% isoflurane. After 4 weeks, mice were sacrificed by cervical dislocation and brain tissue was isolated. To investigate the effects of oxidative stress on AAV/B130-shHtrA1 C57BL/6J mice were intraperitoneally administered GLX351322 (5 mg/kg/day) for 4 weeks.

Tissue immunofluorescence. Brain tissue was fixed in 4% paraformaldehyde in 0.1 M phosphate buffer (pH 7.4) for 24 h at 4˚C. Tissue was sectioned into 15 μm slices on a cryostat (Leica, RM2235). Antigen retrieval was performed by heating the sections in EDTA antigen retrieval solution (Zhongshan Jinqiao Biotechnology Co., Ltd.; cat. no. ZLI-9069) at 95˚C for 2 min in a water bath. After cooling to room temperature, the sections were blocked with 5% BSA (Solarbio, cat. no. SW3015) for 30 min. The sections were incubated with primary antibodies overnight at 4˚C and with the secondary antibodies for 1 h at room temperature. The primary antibodies were as follows: Mouse-anti-α-smooth muscle actin (SMA; Zenbio, Inc.; cat. no. L29JLZC) and rabbit-anti-HtrA1 (both 1:50, Proteintech Group, Inc.; cat. no. 00129131). The secondary antibodies were Alexa Fluor 488-labeled goat anti-mouse (cat. no. A0428) and Alexa Fluor 555-labeled donkey anti-rabbit IgG (H+L; both 1:500, both Beyotime; cat. no. A0453). The nuclei were counterstained with DAPI (Beijing Solarbio Science & Technology Co., Ltd.; C0065) for 10 min at 25˚C. Fluorescent images were captured using a confocal microscope (Leica GmbH).

Evans blue assay. Mice were intravenously injected with 0.5% Evans blue (Absin, cat. no. Abs47002009) in saline at 3 ml/kg body weight and euthanized 2 h after dye circulation. The weight of each cerebral hemisphere was recorded and Evans blue extraction was performed by incubating the brain tissue in acetone for 24 h at 25˚C, followed by centrifugation at 12,000 x g for 30 min at 4˚C. Evans blue staining was quantified by measuring the absorbance at 620 nm using a spectrophotometer (Thermo Fisher Scientific, Inc.).

Open-field test (OFT). Each mouse underwent the OFT once to avoid habituation or stress-associated behavioral changes. A plain 50x50x40 cm open-field arena was used to assess the locomotor activity and anxiety-like behavior. Following 30 sec habituation, the total distance traveled and time spent in the center arena (16.7x16.7 cm) was recorded in a 5 min session. The frequencies of rearing and defecation in the apparatus were recorded. At the end of each experimental trial, the apparatus was thoroughly cleaned and disinfected by spraying 75% ethyl alcohol to eliminate residual olfactory cues. Mouse behavior was analyzed using VisuTrack software (XR-VT version, Shanghai Xinruan Information Technology Co., Ltd.).

Novel object recognition test (NORT). Mice were placed in an open field with two identical objects to familiarize them with their environment. Following 6 h, the mice were returned to the same open field for testing. One of the familiar objects was replaced with a novel object that had a unique color and shape. In both phases of the experiment, each mouse faced the wall of the apparatus and was allowed to explore the objects freely for 5 min. Before each trial, the apparatus was cleaned using 75% ethanol solution. Mouse behavior was recorded using a video tracking system and analyzed using the VisuTrack software. NOR memory was evaluated using the NOR index (NOI) as follows: NOI=(time spent exploring the novel object)/(total exploration time for both objects) x100%.

Morris water maze (MWM) test. The MWM test was conducted in a white circular tank, measuring 120 cm in diameter and 50 cm in height, filled with tap water maintained at 22±3˚C, and divided into four equal virtual quadrants. Non-toxic white paint was added to ensure the water was opaque. During the place navigation-training phase, which consisted of four trials of 120 sec/day over 4 consecutive days, a circular escape platform (diameter, 10 cm) was submerged 1 cm below the water surface in a designated quadrant. Each mouse was released from different starting positions, facing the tank wall and allowed to locate the escape platform. Upon reaching the platform, the mouse was allowed to stay on it for 3 sec. Latency to escape onto the platform was recorded. If a mouse failed to locate the platform within 120 sec, it was guided to the platform and allowed to remain there for 30 sec. On day 5, a probe test was conducted, wherein the mice swam freely without the platform for 120 sec. The proportion of time spent in the target quadrant and the number of platform crossings were recorded. Swimming paths were monitored and analyzed using VisuTrack software.

Statistical analysis. Statistical analysis was performed using the GraphPad Prism 9 (GraphPad Software Inc.; Dotmatics) and R (version 4.3.1; R Foundation for Statistical Computing) software. Data are presented as the mean ± standard deviation of three independent experiments. Comparisons were made using one-way ANOVA followed by Tukey's, LSD t or Dunnett's post hoc test. Differentially expressed genes were analyzed using the DESeq2 package. The Wald test was used to analyze the differences between two groups, with the filtering conditions set at $|\log_2 FC|>1$ and an adjusted P-value <0.05. The significance of enrichment analysis was assessed using a hypergeometric distribution test. P<0.05 was considered to indicate a statistically significant difference.

Results

Sanger sequencing, family pedigree, clinical results and RNA-seq analysis for heterozygous HTRA1mcs. Sanger sequencing was performed to analyze the carrier status of the pathogenic variants in two families (Fig. 1A and B). In family 1 (F1), the proband (F1 III-5), his elder brother (F1 III-1) and younger brother (F1 III-7) were found to carry a heterozygous *HTRA1* mutation (c.854C>T, p.P285L). In F2, the proband (F2 III-1), two sisters (F2 III-2 and -4) and a brother (F2 III-6) carried a heterozygous *HTRA1* mutation (c.905G>A, p.R302Q). The proband (F2 III-1) and their sister (F2 III-2) and brother (F2 III-6) all died of cerebrovascular diseases.

The predicted pathogenicity of the HTRA1 c.854 C>T and c.905 G>A mutations is shown in Table III. The phenotypic characteristics exhibited a notable degree of homogeneity, with the clinical presentation, including subcortical ischemic events and progressive cognitive decline, being characteristic of CSVD (Table IV). The pedigrees of families with heterozygous *HTRA1* mutations are shown in Fig. 1A.

F1III-1 was a 49-year-old male patient who presented with recurrent strokes and cognitive decline for 20 years. The patient experienced a first stroke, manifesting as left-sided weakness and dysphagia. The patient is bedridden because of limb weakness, gait disturbance and pseudobulbar palsy. The patient had a medical history of alopecia and spondylosis deformans. Brain MRI, with fluid-attenuated inversion-recovery (FLAIR) sequences, revealed multiple lacunar infarcts and confluent white matter hyperintensity (WMH) in the periventricular regions (Fig. 1C). Cognitive evaluation at the time of diagnosis demonstrated substantial impairment. The patient achieved a Montreal Cognitive Assessment (MoCA) score of 13/30 (severe impairment; normal range ≥26) and a Mini-Mental State Examination (MMSE) score of 16/30 (moderate impairment; normal range ≥24).

F1III-5 was a 46-year-old male patient who presented with right-sided weakness, dysarthria, history of cerebral infarction, and cognitive decline. The patient had alopecia and spondylosis deformans with lumbar disc surgery. Brain MRI with FLAIR sequences revealed multiple lacunar infarcts and WMH in the periventricular regions (Fig. 1C). Cognitive assessment revealed a notable decline (MoCA score, 15; MMSE score, 18).

F1III-7 was a 44-year-old male patient who presented with recurrent dizziness and gait unsteadiness. The patient exhibited hypertension and diabetes. Brain MRI indicated multiple lacunar infarcts and WMH (Fig. 1C). Cognitive assessment showed a mild decline (MoCA score, 25; MMSE score, 24).

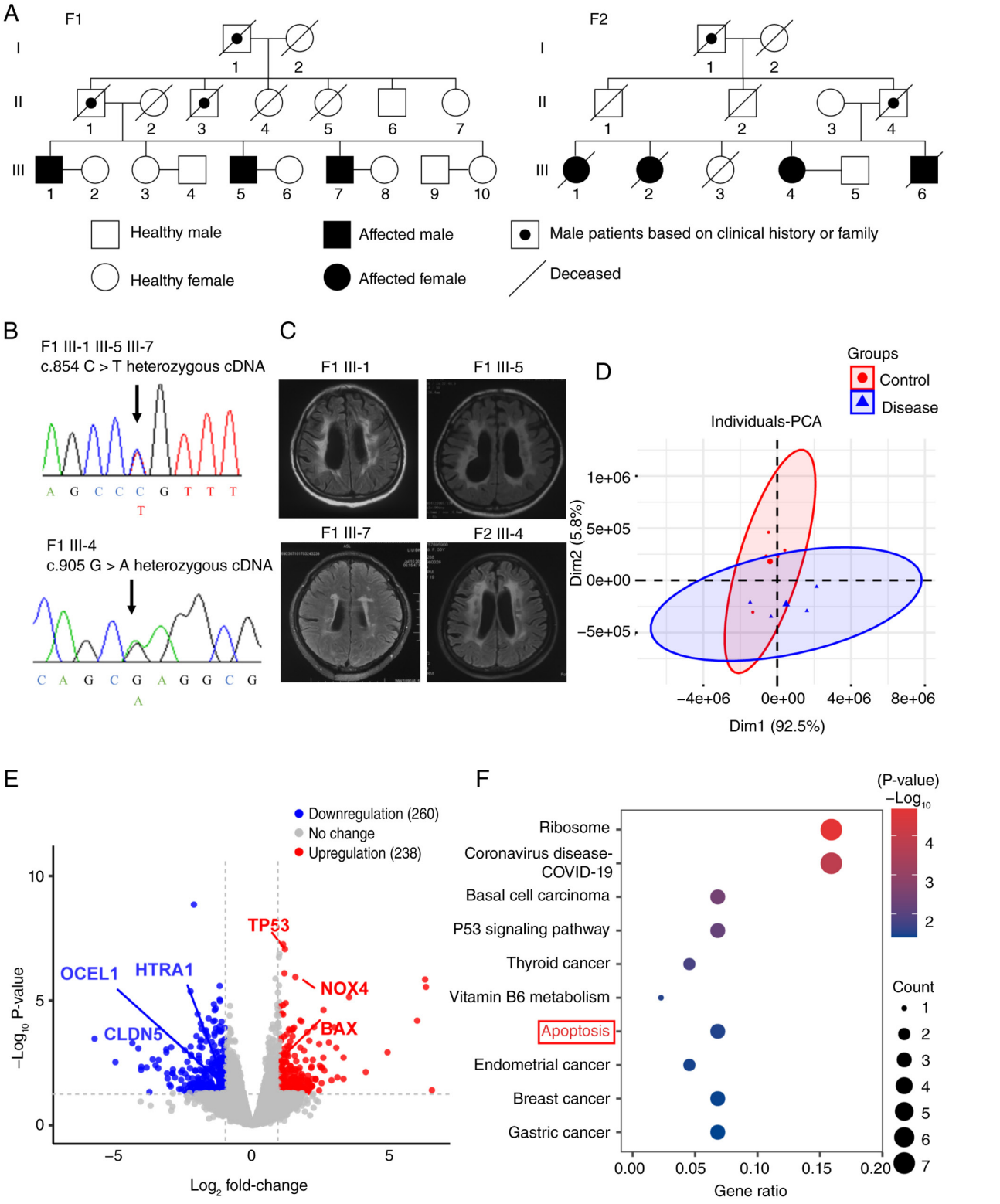

Figure 1. Pedigree of heterozygous *HTRA1* gene mutation carriers, Sanger sequencing and RNA sequencing analysis. (A) Pedigree of heterozygous *HTRA1* gene mutation carriers. (B) Sanger sequencing. Arrows indicate locations of the mutations. (C) Typical neuroimaging of heterozygous *HTRA1* gene mutation carriers. (D) PCA graph showing significant differences between the two sample groups. (E) Volcano plot of differentially expressed genes (log_2 |fold-change|>1, P<0.05). (F) Bubble chart of the Kyoto Encyclopedia of Genes and Genomes pathway enrichment for upregulated genes. 'Apoptosis' was significantly enriched. HTRA1, high temperature requirement serine peptidase A1; OCEL1, occludin-like protein 1; CLDN, claudin5; PCA, principal component analysis; F, family; Dim, dimension.

F2III-4 was a 54-year-old female patient who presented with recurrent dizziness, diplopia and impaired movement of the right limbs, with a history spanning 8 years. Brain MRI showed multiple subcortical lacunar infarcts and WMH (Fig. 1C), with cognitive assessment indicating a mild decline (MoCA score, 23; MMSE score, 21).

Table III. Predicted pathogenicity of the HTRA1 c.854 C>T and c.905 G>A mutations.

Variant	Protein domain	ID SNP	Polyphen-2	SIFT	Mutation taster	CADD	nsSNP analyzer	Mutation assessor
c.854 C>T (p.P285L)	Serine protease	rs587776446	Probably damaging	Damaging (score, 0.016)	Disease-causing	Deleterious	Disease	Medium functional impact
c.905 G>A (p.R302Q)	Serine protease	rs2133449474	Probably damaging	Damaging (score, 0.015)	Disease-causing	Deleterious	Disease	Medium functional impact

HTRA1, high temperature requirement serine peptidase A1; nsSNP, nonsynonymous single nucleotide polymorphism; SIFT, sorting intolerant from tolerant; CADD, combined annotation dependent depletion.

Table IV. Clinical features of heterozygous high temperature requirement serine peptidase A1 mutation carriers.

	Patient			
Characteristic	F1 III-1	F1 III-5	F1 III-7	F2 III-4
Mutation	p.P285L	p.P285L	p.P285L	p.R302Q
Sex	Male	Male	Male	Female
Age, years	49	46	44	54
Age at first stroke episode, years	35	41	42	48
Gait disturbance	Present	Present	Absent	Present
Cognitive decline	Present	Present	Present	Present
Spondylosis deformans	Present	Present	Absent	Absent
Alopecia	Present	Present	Present	Absent
Hypertension	Absent	Absent	Present	Absent
Diabetes mellitus	Absent	Absent	Present	Absent
Dyslipidemia	Absent	Absent	Absent	Absent
Pseudobulbar palsy	Present	Present	Absent	Absent
Hyperreflexia of limbs	Present	Present	Absent	Present
Babinski reflex	Present	Present	Present	Present
Chronic heart failure	Absent	Absent	Absent	Absent
Heavy alcohol consumption	Absent	Absent	Absent	Absent
Smoking	Absent	Absent	Absent	Absent

F, family.

PCA revealed significant differences between the HTRA1mc and HC groups (Fig. 1D). In total, 489 differentially expressed genes were identified, of which 238 were up- and 260 were downregulated (Figs. 1E and 2A). In the HTRA1mc group, mRNA expression of *HTRA1*, occludin-like protein 1 (*OCEL1*) and *CLDN5* was downregulated, whereas that of *NOX4* and Bcl-2 associated X (*BAX*) was upregulated (Fig. 1E). The KEGG enrichment analysis showed significant enrichment in 'ribosome', 'P53 signaling pathway', 'apoptosis', 'thyroid cancer', 'endometrial cancer', 'breast cancer', and gastric cancer (Fig. 1F). GO enrichment analysis revealed significant enrichment in 'defense response to virus', 'leukocyte-mediated immunity', 'lymphocyte mediated immunity', and 'cell killing' (Fig. 2B). The HTRA1mc group showed decreased plasma HTRA1 (Fig. 2C) and elevated NOX4 protein (Fig. 2D) levels compared with the HC group. These findings indicated that *HTRA1* mutations may increase oxidative stress and apoptosis, thereby contributing to CSVD. Additionally, the downregulation of tight junction-associated genes, such as *OCEL1* and *CLDN5*, may impair the blood-brain barrier (BBB) function.

Effect of HtrA1 OE on the viability and oxidative stress of bEnd.3 cells. mCherry red fluorescence carried by lentivirus was observed in both the NC-OE and HtrA1-OE groups (Fig. 3A). RT-qPCR and western blot analyses showed that the *HtrA1* mRNA (Fig. 3B) and protein (Fig. 3C) levels were significantly higher in the HtrA1-OE group than in the NC-OE

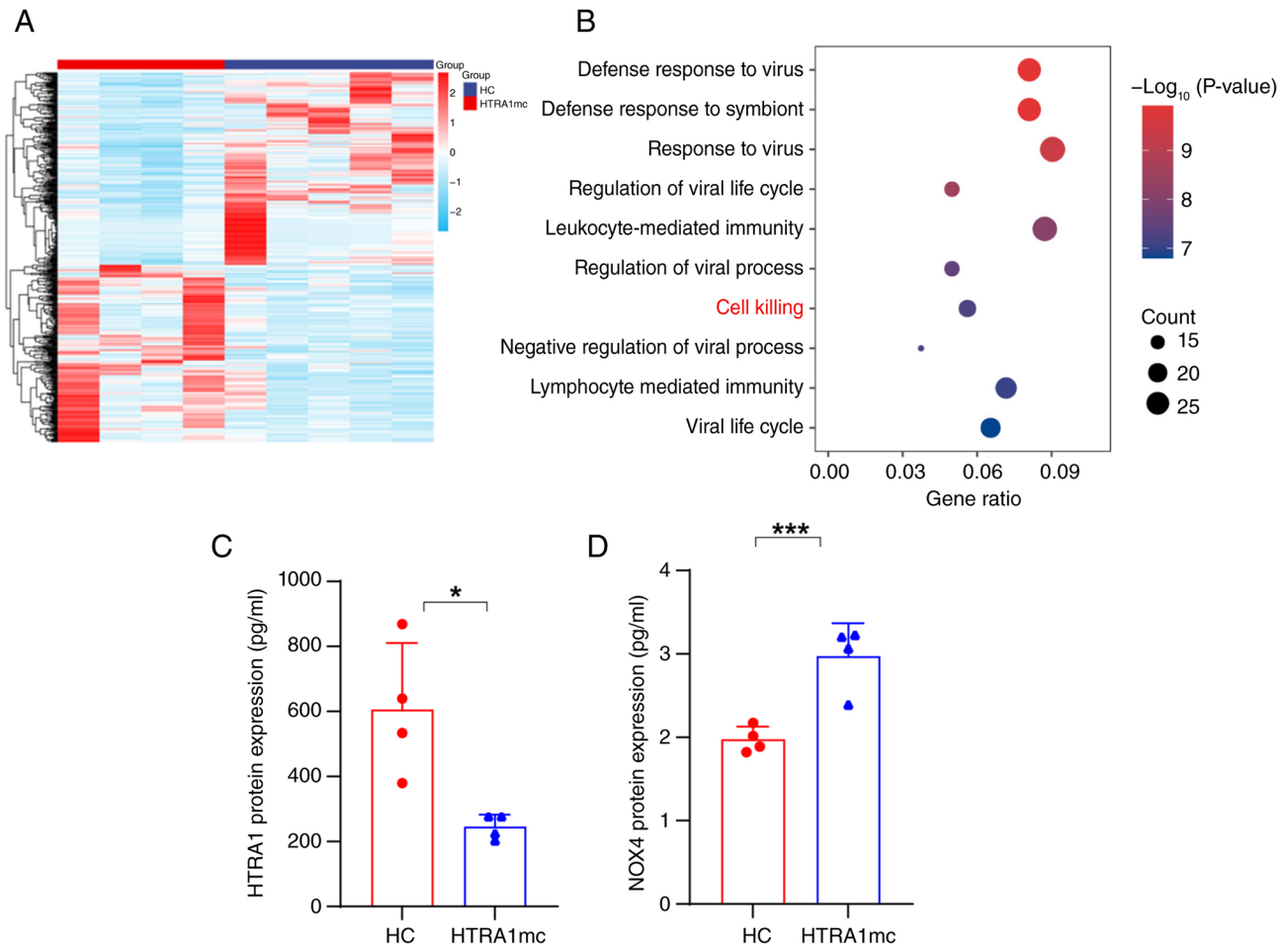

Figure 2. RNA sequencing of differentially expressed genes and plasma expression. (A) Hierarchical clustering heatmap of differentially expressed genes. (B) Bubble plot illustrating Gene Ontology enrichment of differentially expressed genes. Plasma (C) HTRA1 and (D) NOX4 expression levels between heterozygous HTRA1mcs and HCs were determined using ELISA. *P<0.05, ***P<0.001. HTRA1mc, high temperature requirement serine peptidase A1 mutation carrier; HC, healthy control.

group. No differences were observed between the UT-OE and NC-OE groups (Fig. 3B and C). In the CCK-8 assay, cells in the HtrA1-OE group exhibited enhanced viability at both 48 and 72 h compared with those in the NC-OE group (Fig. 3D). These findings were supported by the RTCA results (Fig. 3E), which suggested that HtrA1 OE improved the viability of bEnd.3 cells. DCFH-DA, SOD and MDA assays were performed to assess oxidative stress. The HtrA1-OE group showed decreased NOX4 expression (Fig. 3C and F) and reactive oxygen species (ROS) levels (Fig. 3G) compared with the NC-OE group, whereas the SOD activity was higher and MDA levels were lower in the HtrA1-OE group (Fig. 3H). These results indicated that HtrA1 OE decreased oxidative stress and exerted a protective effect on bEnd.3 cells.

Effect of HtrA1 OE on tight junctions, permeability and apoptosis in bEnd.3 cells. HtrA1 OE in bEnd.3 cells significantly increased the expression of tight junction proteins ZO1, occludin and CLDN5 in the HtrA1-OE group compared with that in the NC-OE group (Fig. 4A). These results were corroborated by immunofluorescence, with higher expression levels of these proteins observed in the HtrA1-OE group (Fig. 4B and C). The FITC-dextran experiment revealed decreased cell permeability in the HtrA1-OE group compared with that in the NC-OE group (Fig. 4D), indicating strengthened tight junctions. Western blotting revealed a significant decrease in caspase3 expression in the HtrA1-OE group compared with that in the NC-OE group (Fig. 4E). Flow cytometry also indicated decreased apoptosis in the HtrA1-OE group compared with the NC-OE group (Fig. 4F). These findings indicated that HtrA1 OE strengthened the integrity of tight junctions and decreased apoptosis in bEnd.3 cells.

Effects of HtrA1 knockdown on bEnd.3 cell viability and oxidative stress. Both the sh-NC and sh-HtrA1 groups showed green fluorescence, confirming successful establishment of a stable HtrA1 knockdown cell line (Fig. 5A). RT-qPCR and western blot analyses revealed significantly decreased *HtrA1* mRNA and protein levels in the shRNA-HtrA1-mus-1079 group compared with those in the sh-NC group (Fig. 5B and C). As the shRNA-HtrA1-mus-1079 group showed the highest interference efficiency, it was selected as the sh-HtrA1 group for subsequent experiments. The CCK-8 assay showed decreased viability of cells in the sh-HtrA1 group at 72 h compared with that in the sh-NC group (Fig. 5D). Consistently, RTCA (Fig. 5E) demonstrated decreased cell viability following HtrA1 knockdown. The expression of NOX4 was increased in the sh-HtrA1 group compared with that in the sh-NC group, as

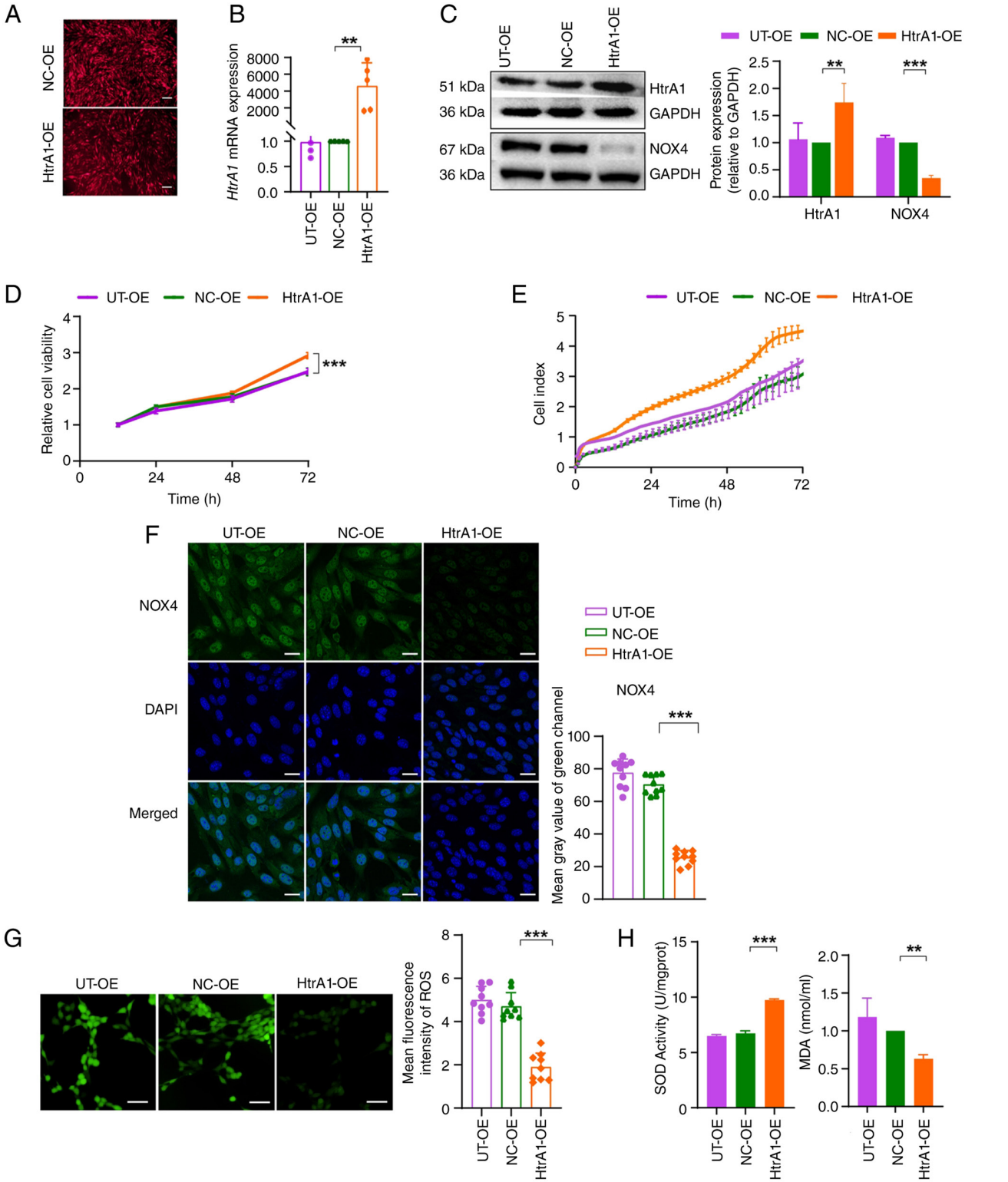

Figure 3. Effect of lentiviral vector-mediated HtrA1 OE on bEnd.3 cell viability and oxidative stress. (A) Infection with lentiviral supernatant induced OE of HtrA1 in bEnd.3 cells. Scale bar, 200 μm. (B) Reverse transcription-quantitative PCR analysis of *HtrA1* mRNA expression in bEnd.3 cells. (C) Western blot analysis of HtrA1 and NOX4 protein expression in bEnd.3 cells. (D) Cell viability evaluated using the Cell Counting Kit-8 assay. (E) Real-time monitoring of cell viability in each group using real-time cellular analysis. (F) Immunofluorescence staining of NOX4 (green) and cell nuclei (blue) in bEnd.3 cells. Scale bar, 25 μm. (G) DCFH-DA analysis of intracellular ROS. Scale bar, 100 μm. (H) Activity of SOD and concentration of MDA in bEnd.3 cells. **P<0.01, ***P<0.001. HtrA1, high temperature requirement serine peptidase A1; OE, overexpression; SOD, superoxide dismutase; MDA, malondialdehyde; UT, untransfected; NC, negative control; ROS, reactive oxygen species.

evidenced by western blot analysis (Fig. 5F) and immunofluorescence (Fig. 5G). ROS levels were higher in the sh-HtrA1 group compared with sh-NC group (Fig. 5H), whereas the SOD activity and MDA levels were lower and higher, respectively (Fig. 5I). These findings indicated that HtrA1 knockdown increased oxidative stress in bEnd.3 cells.

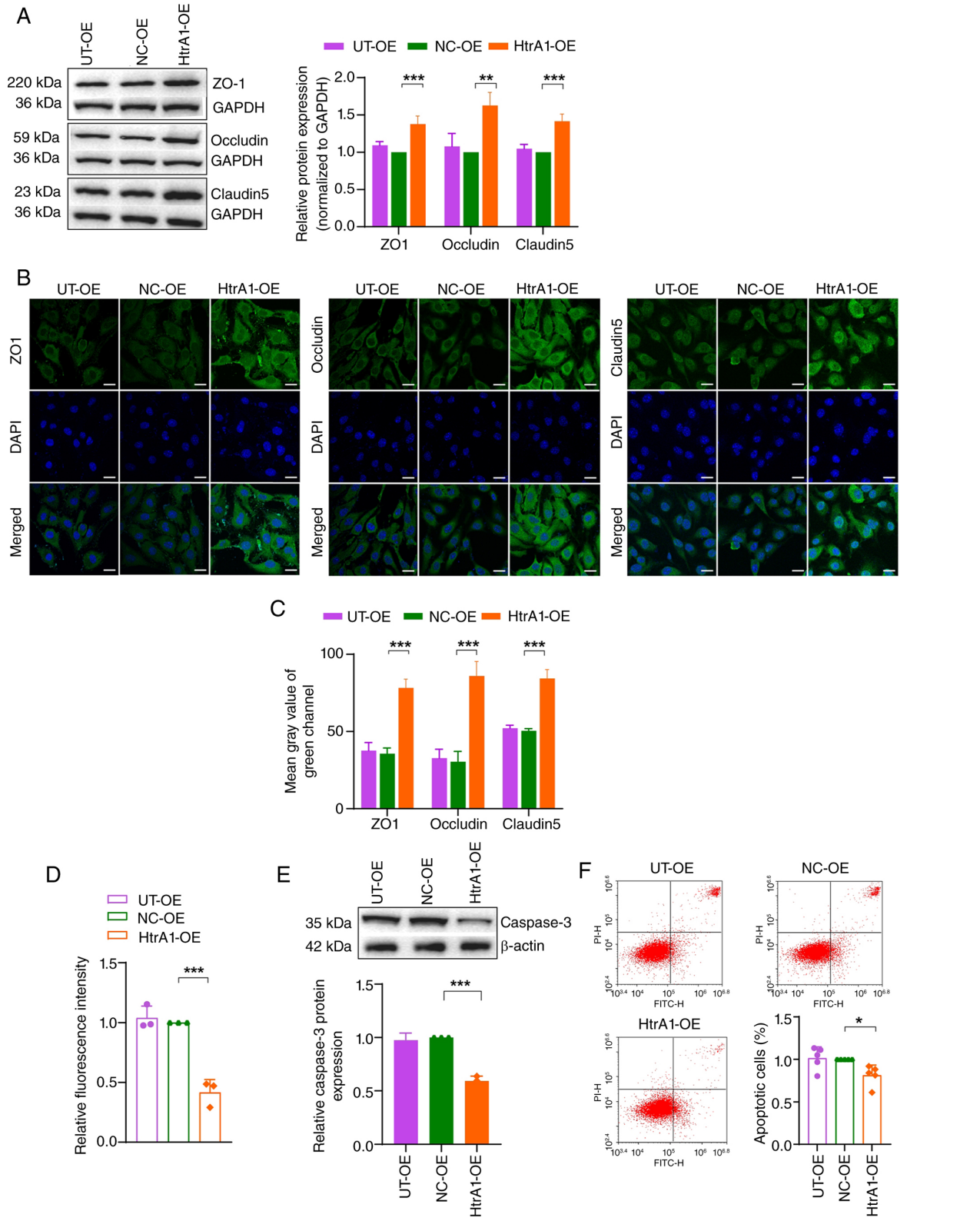

Figure 4. Effect of HtrA1 OE on tight junctions, permeability and apoptosis in bEnd.3 cells. (A) Western blot analysis of ZO1, occludin and claudin 5 proteins in bEnd.3 cells. (B) Immunofluorescence of ZO1, occludin, claudin 5 and nuclei (blue) in bEnd.3 cells. Scale bar, 25 μm. (C) Mean gray value of green channel of ZO1, occludin and claudin 5. (D) Permeability of bEnd.3 cell monolayers was assessed using FITC-dextran. (E) Western blot analysis of caspase3 protein in bEnd.3 cells. (F) Flow cytometry analysis of bEnd.3 cell apoptosis. *P<0.05, **P<0.01, ***P<0.001. HtrA1, high temperature requirement serine peptidase A1; OE, overexpression; ZO1, zonula occludens protein 1; UT, untransfected; NC, negative control.

Effect of HtrA1 knockdown on tight junction, permeability and apoptosis in bEnd.3 cells. Following HtrA1 knockdown in bEnd.3 cells, western blot analysis showed decreased expression of the tight junction proteins ZO1, occludin and CLDN5 in the sh-HtrA1 group compared with that in the sh-NC group (Fig. 6A). Confocal microscopy confirmed this

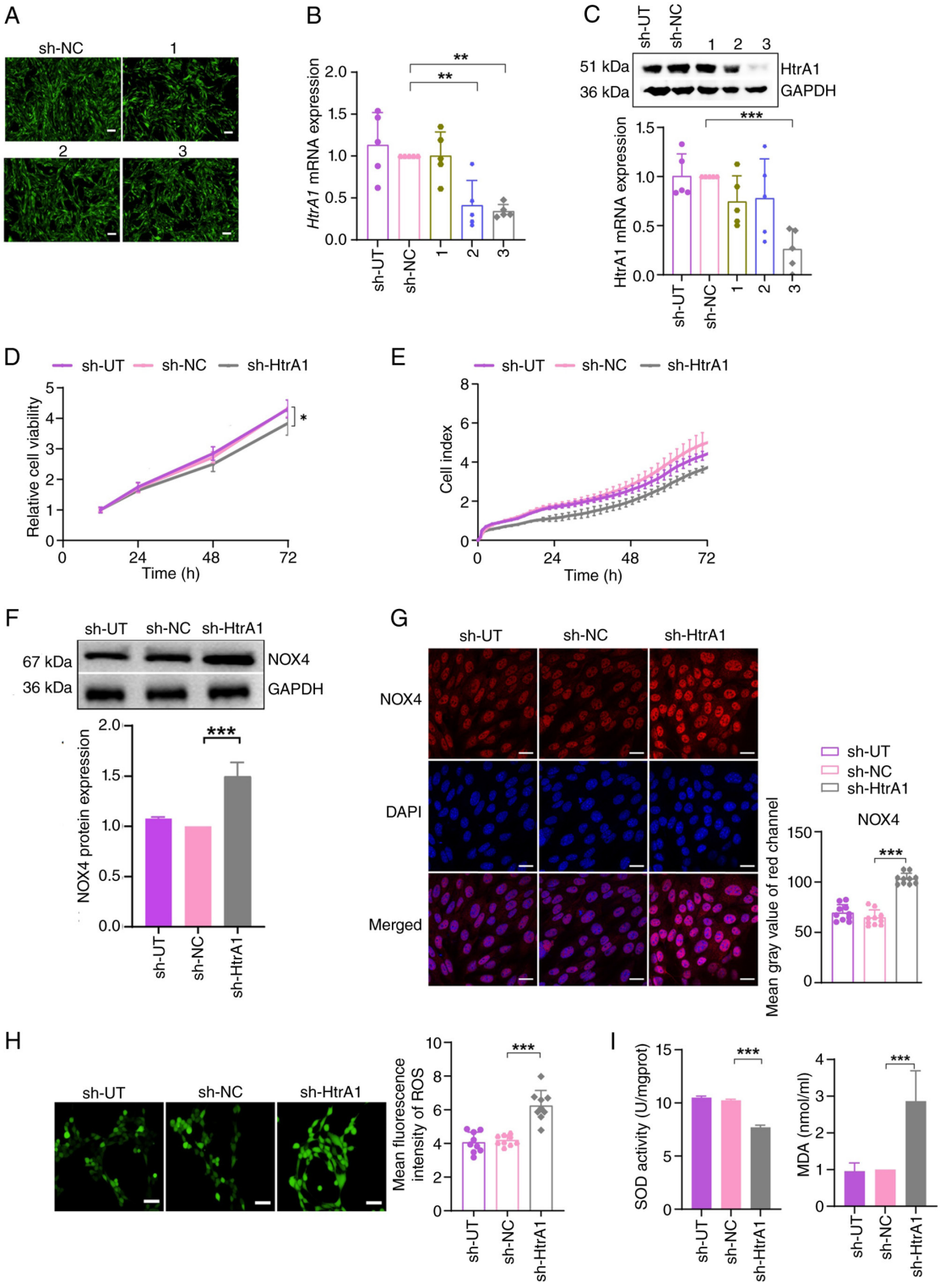

Figure 5. Effect of lentiviral vector-mediated HtrA1 knockdown on bEnd.3 cell viability and oxidative stress. (A) Infection with lentiviral supernatant induced knockdown of HtrA1 in bEnd.3 cells. Scale bar, 200 μm. (B) Reverse transcription-quantitative PCR analysis of HtrA1 mRNA expression. (C) Western blot analysis of HtrA1 protein expression in bEnd.3 cells. (D) Cell viability was evaluated using Cell Counting Kit-8 assay. (E) Real-time monitoring of cell viability using real-time cellular analysis. (F) Western blot analysis of NOX4 protein expression in bEnd.3 cells. (G) Immunofluorescence analysis of NOX4 (red) and cell nuclei (blue) in bEnd.3 cells. Scale bar, 25 μm. (H) DCFH-DA staining showing intracellular ROS levels. Scale bar, 100 μm. (I) Activity of SOD and concentration of MDA in bEnd.3 cells. *P<0.05, **P<0.01, ***P<0.001. 1, shRNA-HtrA1-mus749; 2, shRNA-HtrA1-mus885; 3, shRNA-HtrA1-mus1079; HtrA1, high temperature requirement serine peptidase A1; ROS, reactive oxygen species; SOD, superoxide dismutase; MDA, malondialdehyde; sh, short hairpin; UT, untransfected; NC, negative control.

reduction (Fig. 6B and C). The FITC-dextran assay revealed increased permeability in the sh-HtrA1 group (Fig. 6D), indicating compromised tight junction integrity and enhanced cell permeability following HtrA1 knockdown. Western blot analysis revealed elevated levels of caspase3 in the sh-HtrA1 group compared with the sh-NC group (Fig. 6E). Flow cytometry confirmed increased apoptosis in the sh-HtrA1 group (Fig. 6F). These findings indicated that HtrA1 knockdown

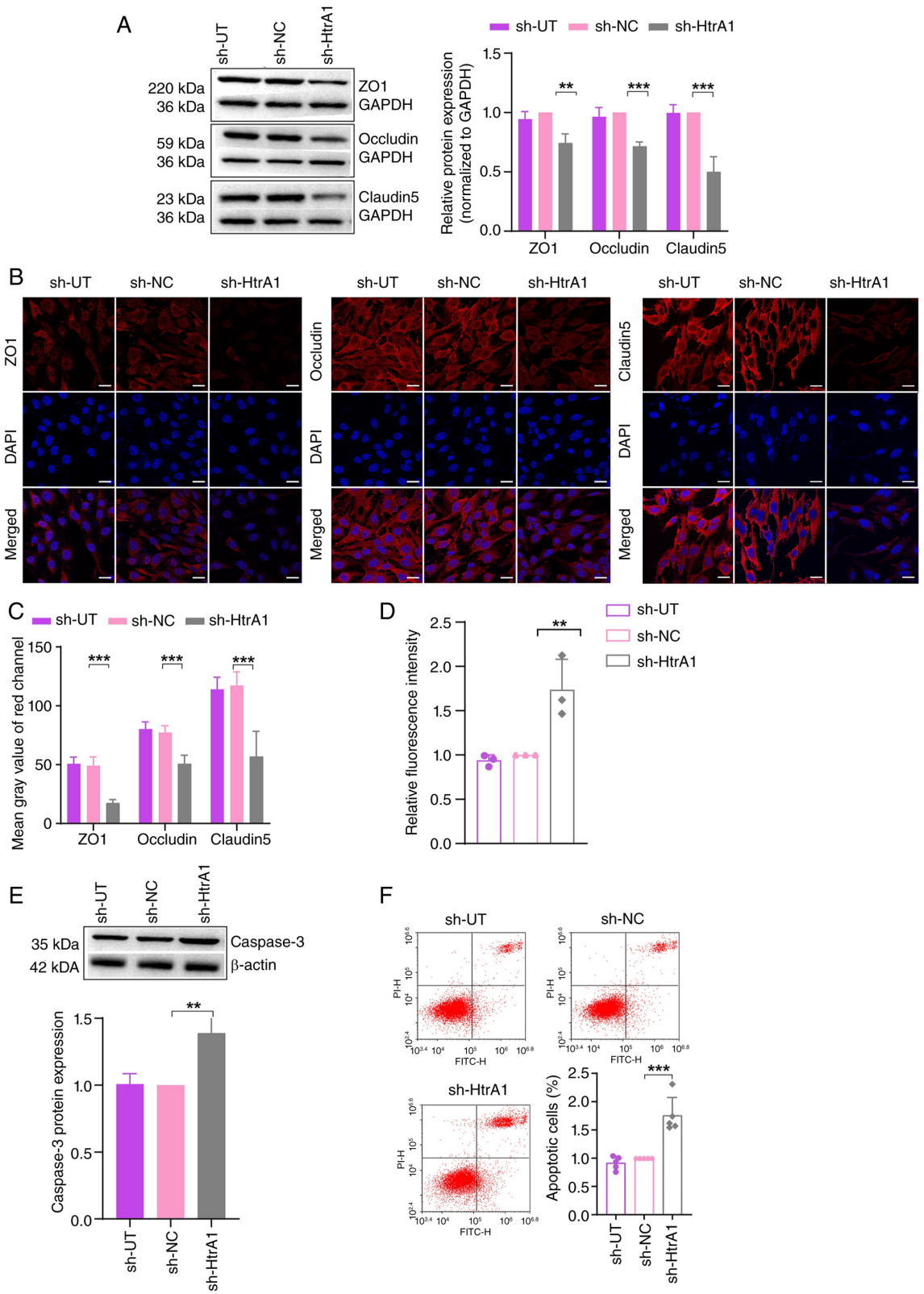

Figure 6. Effect of HtrA1 knockdown on tight junctions, permeability and apoptosis in bEnd.3 cells. (A) Western blot analysis of ZO1, occludin and claudin 5 proteins in bEnd.3 cells. (B) Immunofluorescence analysis of ZO1, occludin, claudin 5 and nuclei (blue) in bEnd.3 cells. Scale bar, 25 μm. (C) Quantitative fluorescence analysis. (D) Permeability of bEnd.3 cell monolayers was assessed using FITC-dextran. (E) Western blot analysis of caspase3 proteins in bEnd.3 cells. (F) Flow cytometry analysis of bEnd.3 cell apoptosis. **P<0.01, ***P<0.001. HtrA1, high temperature requirement serine peptidase A1; ZO1, zonula occludens protein 1; sh, short hairpin; UT, untransfected; NC, negative control.

increased apoptosis in bEnd.3 cells, emphasizing the role of HtrA1 in regulating tight junctions and cell barrier properties.

Interference with HtrA1 expression in cerebral vascular endothelial cells of C57BL/6J mice. An endothelial cell-specific HtrA1 knockdown mouse model was constructed by injecting

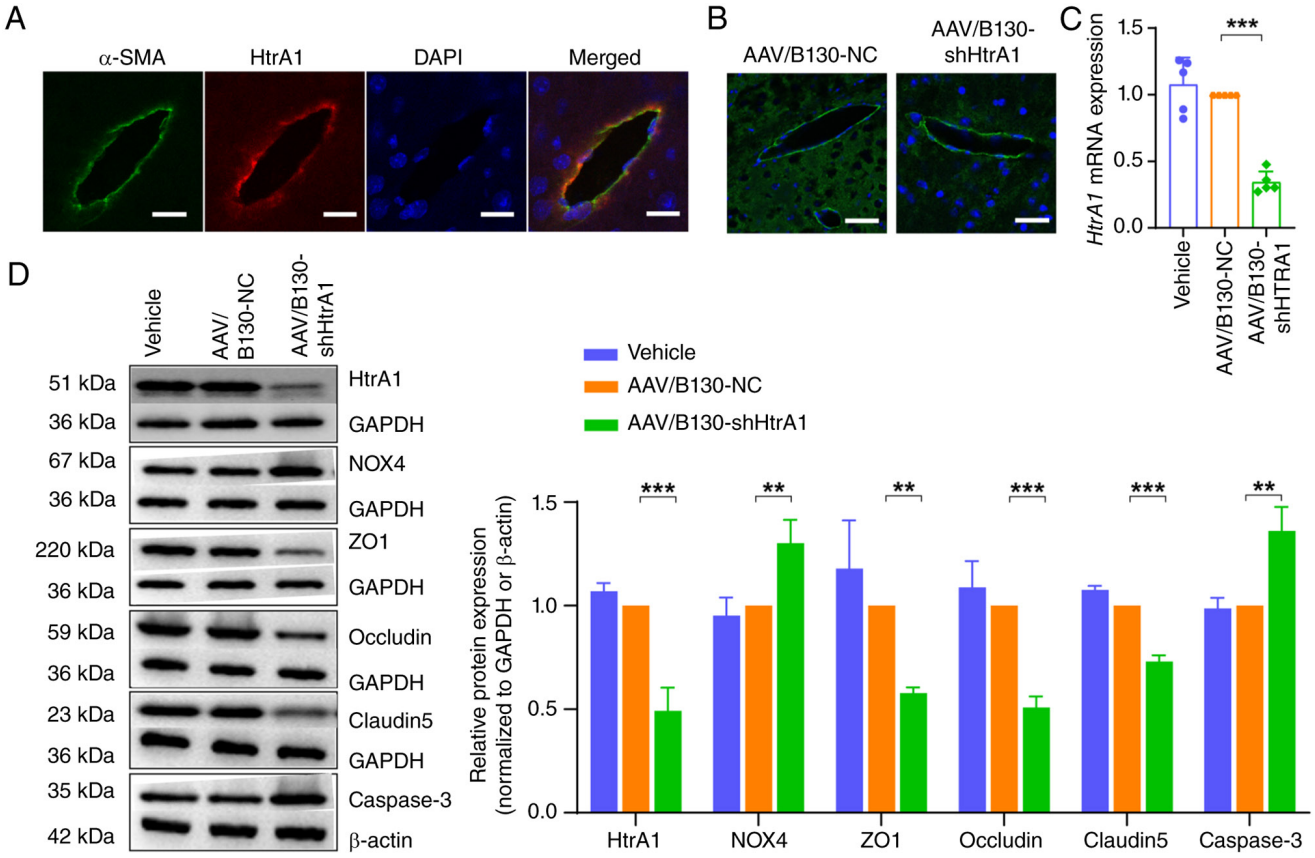

Figure 7. Interference with HtrA1 expression in cerebral vascular endothelial cells of C57BL/6J mice. (A) Mouse cerebral vascular endothelial cells showing HtrA1 expression colocalized with the expression of vascular marker α-SMA. (B) AAV2/B130-TIE was injected into the tail vein of C57BL/6J mice. Scale bar, 25 μm. (C) Reverse transcription-quantitative PCR analysis of HtrA1 mRNA expression in the brain tissue of C57BL/6J mice. (D) Western blot analysis of HtrA1, NOX4, ZO1, occludin, claudin 5 and caspase3 protein in the brain tissue of C57BL/6J mice. **P<0.01, ***P<0.001. HtrA1, high temperature requirement serine peptidase A1; SMA, smooth muscle actin; AAV, adeno-associated virus; ZO1, zonula occludens protein 1; sh, short hairpin; NC, negative control.

AAV2/B130-TIE carrying a specific endothelial promoter into the tail vein of C57BL/6J mice. After 4 weeks, immunofluorescence staining of HtrA1 in mouse brain slices showed notable HtrA1 expression in cerebrovascular endothelial cells, colocalizing with the vascular marker α-SMA (Fig. 7A). The green fluorescent protein marker in the viral vector confirmed the successful transfection of endothelial cells (Fig. 7B). RT-qPCR and western blotting revealed significantly reduced *HtrA1* mRNA (Fig. 7C) and protein levels (Fig. 7D) in the AAV/B130-shHtrA1 group, indicating effective gene knockdown. Expression of tight junction proteins ZO1, occludin and CLDN5 decreased, whereas that of NOX4 and caspase3 was increased in the AAV/B130-shHtrA1 compared with that in the AAV/B130-NC group (Fig. 7D).

HtrA1 regulates tight junctions, permeability and apoptosis of brain vascular endothelial cells via the NOX4-dependent oxidative stress pathway. Functional rescue experiments using GLX351322 were performed following HtrA1 knockdown in bEnd.3 cells. The sh-HtrA1 + GLX351322 group exhibited a significant decrease in NOX4 expression compared with the sh-NC group (Fig. 8A). The present study evaluated expression levels of tight junction proteins, ZO1, occludin and CLDN5. Western blot analysis did not indicate any significant differences between the sh-HtrA1 + GLX351322 and sh-NC groups (Fig. 8A). In the FITC-dextran experiment, no significant increase in permeability was observed for the sh-HtrA1 + GLX351322 compared with the sh-NC group (Fig. 8B). There was no significant difference in levels of caspase3 in the sh-HtrA1 + GLX351322 compared with the sh-NC group (Fig. 8A). Moreover, flow cytometry showed that the apoptosis rate in the sh-HtrA1 + GLX351322 group was similar to that in the sh-NC group (Fig. 8C). These findings indicated that inhibiting NOX4 expression enhanced the expression of tight junction proteins, decreased cell permeability and mitigated apoptosis. Western blot analysis (Fig. 8D) showed elevated protein expression of NOX4 in the AAV/B130-shHtrA1 compared with the AAV/B130-NC mice. GLX351322 treatment significantly decreased the NOX4 levels, indicating effective inhibition. Additionally, GLX351322 increased the expression of tight junction proteins ZO1, occludin and CLDN5 and decreased the expression of caspase3 compared with that in the AAV/B130-shHtrA1 group. The Evans Blue assay revealed decreased BBB permeability following GLX351322 injection (Fig. 8E).

Intraperitoneal injection of GLX351322 attenuates immobility and anxiety in AAV/B130-shHtrA1 mice. In the OFT, the AAV/B130-shHtrA1 mice exhibited significantly decreased total distance traveled and decreased time spent in the central region compared with the AAV/B130-NC mice (Fig. 9A-C).

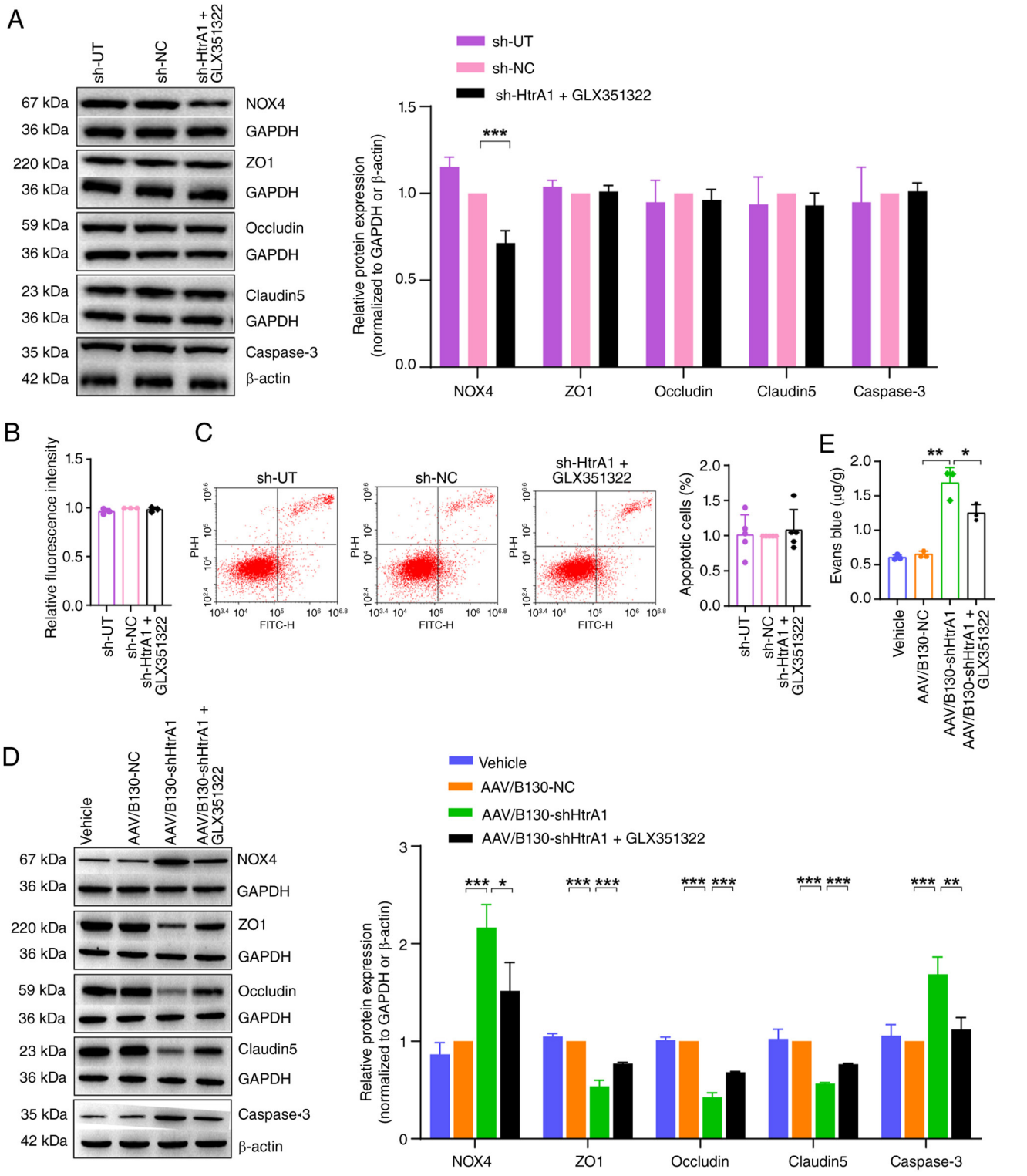

Figure 8. HtrA1 regulates tight junctions, permeability and apoptosis of brain vascular endothelial cells via the NOX4-dependent oxidative stress pathway. (A) Western blot analysis of NOX4, ZO1, occludin, claudin 5 and caspase3 protein expression in bEnd.3 cells. (B) Permeability of bEnd.3 cell monolayers was assessed using FITC-dextran. (C) Flow cytometry analysis of bEnd.3 cell apoptosis. (D) Western blot analysis of NOX4, ZO1, occludin, claudin 5 and caspase3 in the mouse brain tissue. (E) Blood-brain barrier permeability of the mouse brain tissue was determined using Evans blue assay. *P<0.05, **P<0.01, ***P<0.001. HtrA1, high temperature requirement serine peptidase A1; ZO1, zonula occludens protein 1; sh, short hairpin; UT, untransfected; NC, negative control.

However, GLX351322 significantly increased the total distance travelled and increased time spent in the central region in the AAV/B130-shHtrA1 mice (Fig. 9A-C). AAV/B130-shHtrA1 mice showed decreased rearing and increased defecation frequency compared with the AAV/B130-NC mice (Fig. 9D and E). By contrast, the AAV/B130-shHtrA1 + GLX351322 mice exhibited increased rearing and decreased defecation frequency (Fig. 9D and E). These results indicated that GLX351322 effectively reversed depressive immobility and anxiety in the AAV/B130-shHtrA1 mice.

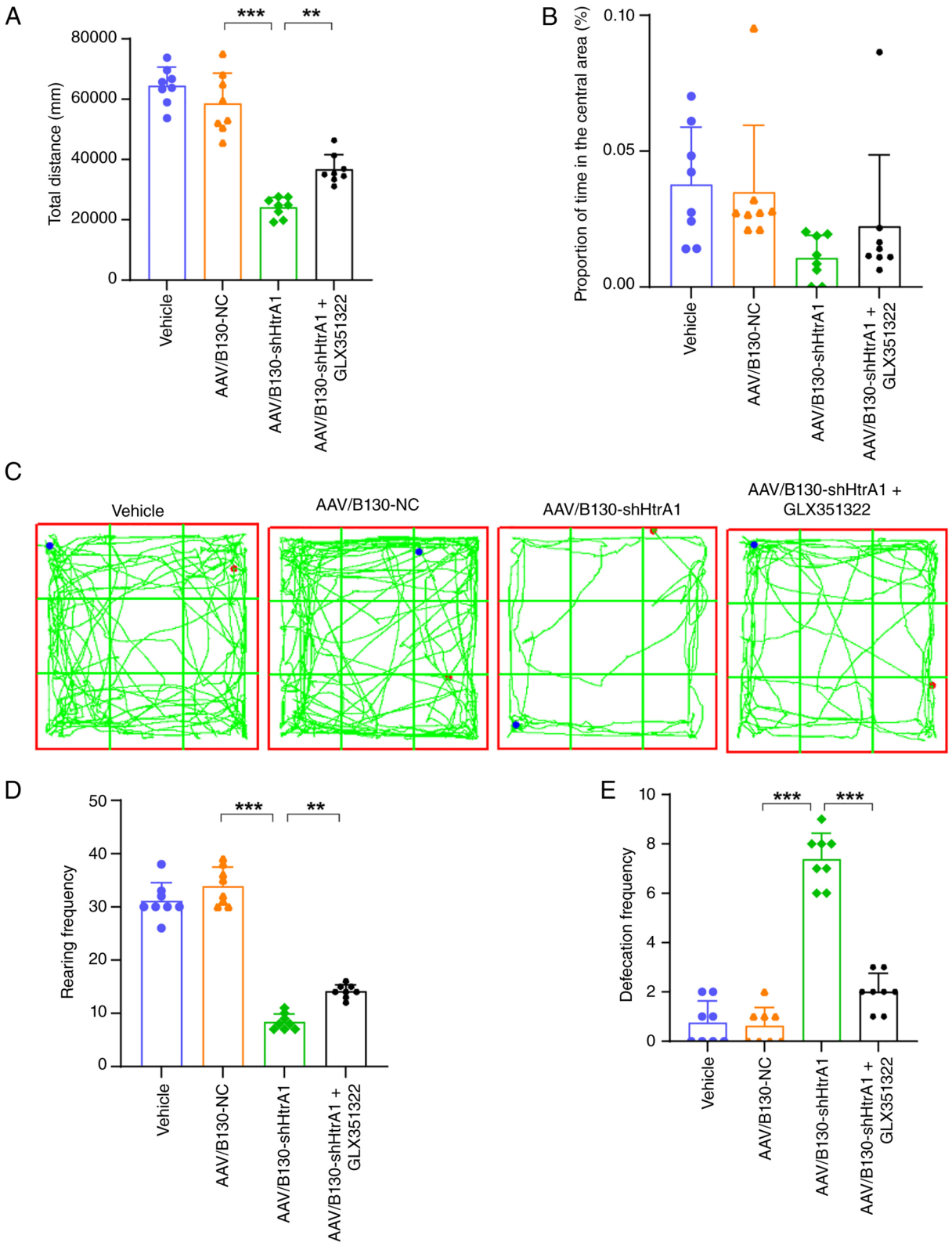

Figure 9. OFT. (A) Histogram of the total distance traveled in the OFT. (B) Percentage of time spent by mice moving in the central area. (C) Representative movement trajectories. (D) Rearing frequency in the OFT. (E) Defecation frequency in the OFT. **P<0.01, ***P<0.001. OFT, open-field test; AAV, adeno-associated virus; HtrA1, high temperature requirement serine peptidase A1; sh, short hairpin; NC, negative control.

Intraperitoneal injection of GLX351322 ameliorates recognition and spatial memory deficit in AAV/B130-shHtrA1 mice. In the NORT (Fig. 10A), no significant difference in the exploration time for two identical objects during the familiarization period was observed between groups (Fig. 10B). During the test phase, the NOI in AAV/B130-shHtrA1 mice was significantly lower than that in AAV/B130-NC mice, whereas intraperitoneal injection of GLX351322 reversed this decline (Fig. 10C).

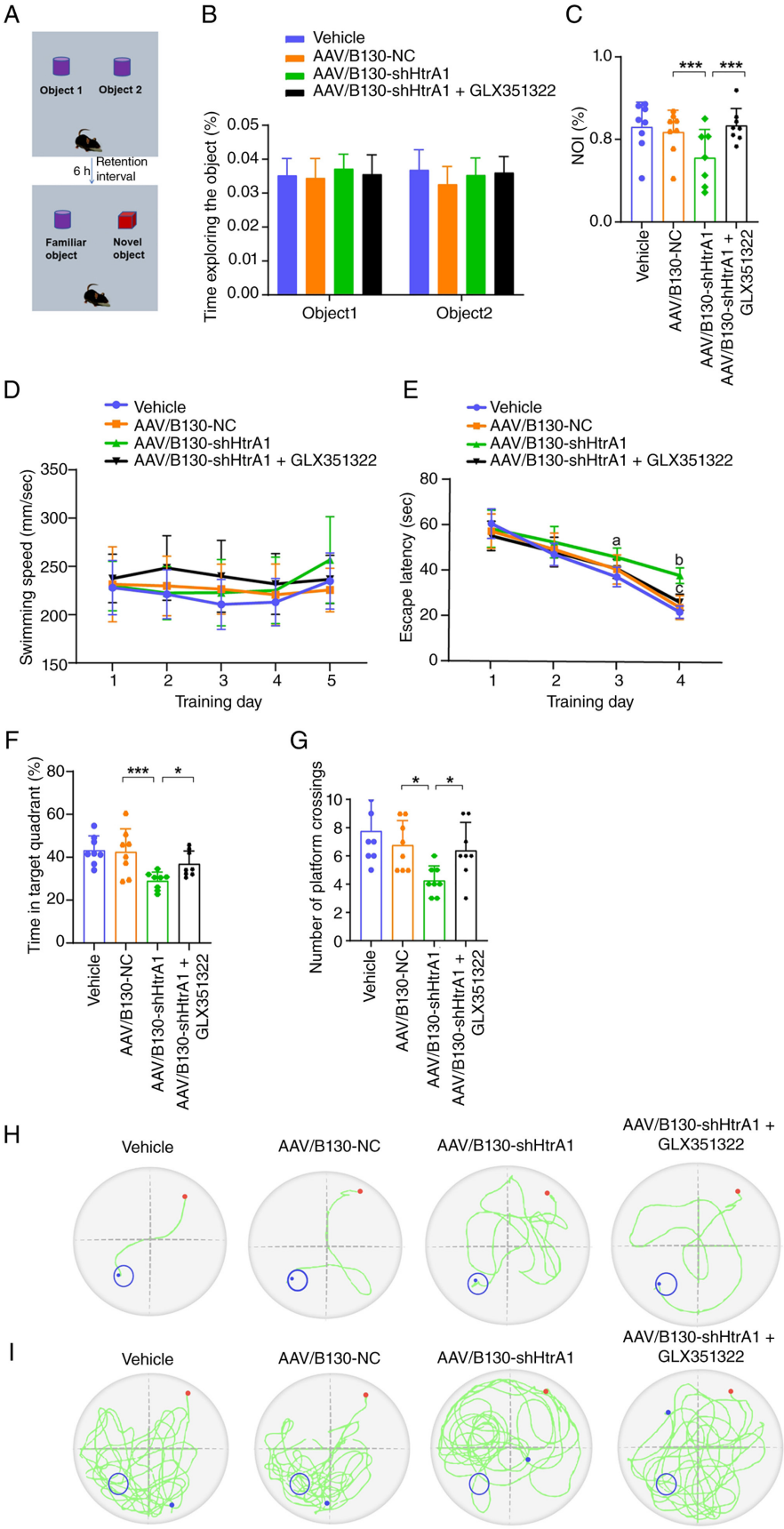

Figure 10. Intraperitoneal injection of the NOX4 inhibitor GLX351322 improves impaired recognition and spatial learning memory in AAV/B130-shHtrA1 mice. (A) Schematic of the NORT. (B) Percentage of time spent exploring two identical objects during the familiarization phase. (C) NOI during the test phase of the NORT. (D) Change in the mean swimming speed of mice during the Morris water maze test. (E) Changes in the escape latency of mice to find the hidden platform during the place navigation training phase. (F) Histograms showing the percentage of swimming time spent in the target quadrant. (G) Histograms showing the number of platform crossings in the probe test. Representative trajectories for each group on (H) training day 4 and (I) probe test. *P<0.05, ***P<0.001. AAV, adeno-associated virus; sh, short hairpin; HtrA1, high temperature requirement serine peptidase A1; NORT, novel object recognition test; NOI, novel object recognition index; NC, negative control.

These results indicated that the intraperitoneal injection of GLX351322 rescued memory deficit in the AAV/B130-shHtrA1 mice. MWM test was used to evaluate spatial learning and memory in mice. No difference in mean swimming speed was observed between the groups during the entire MWM test (Fig. 10D). The escape latency of AAV/B130-shHtrA1 mice was markedly longer on training days 3 and 4 than that of the AAV/B130-NC group, whereas the intraperitoneal injection of GLX351322 significantly shortened the escape latency of AAV/B130-shHtrA1 mice on day 4 during the place navigation-training phase (Fig. 10E), indicating GLX351322 relieved the spatial learning deficit in AAV/B130-shHtrA1 mice. In the probe test, the AAV/B130-shHtrA1 mice demonstrated significantly decreased percentage of swimming time in the target quadrant (Fig. 10F) and number of platform crossings (Fig. 10G) compared with the AAV/B130-NC mice, whereas these decreases were reversed in AAV/B130-shHtrA1 + GLX351322 mice, indicating GLX351322 proficiently improved the spatial reference memory in AAV/B130-shHtrA1 mice. Representative trajectories on training day 4 (Fig. 10H) and during the probe test (Fig. 10I) are shown.

Discussion

In F1, patients exhibited clinical features typical of CSVD, consistent with clinical manifestations of *HTRA1* mutations reported in the literature (25,26). Moreover, the symptoms in patients from F2 also support the role of *HTRA1* mutations in the pathogenesis of CSVD (20). In the present study, the heterozygous *HTRA1* mutations were predicted to be pathogenic. These findings are consistent with previous studies indicating that *HTRA1* heterozygous mutations result in the loss of protein function, triggering extracellular matrix accumulation, cerebrovascular and retinal vascular degeneration and white matter lesions (27,28). RNA-seq results showed significant differences in the expression of genes between heterozygous *HTRA1*mcs and HCs, supporting the existing literature on the crucial role of HTRA1 in cellular signaling and its regulation of physiological functions (29,30). The present study found significant changes in the gene expression of genes associated with oxidative stress and apoptosis in HTRA1mcs compared with HCs. mRNA levels of *NOX4*, a key oxidative stress marker, and *BAX*, a key indicator of apoptosis, were upregulated in the HTRA1mcs. Conversely, the expression of mRNAs encoding tight junction proteins was significantly downregulated. These findings indicated that a disruption in the integrity of the tight junctions may contribute to the pathophysiology of CVSD. Functional analyses, including KEGG pathway analysis, revealed significant enrichment in 'apoptosis'. Collectively, these data indicated that the dysregulation of apoptosis signaling may serve a key role in the disease process. This may be associated with the cerebral microbleeds affected by heterozygous *HTRA1* mutations (31). These results suggest heterozygous *HTRA1* mutations not only affect HTRA1 expression but may also influence cell survival and function by regulating downstream signaling pathways.

Previous studies have indicated that endothelial dysfunction, oxidative stress and apoptosis are key factors contributing to the development of CSVD (32-34). HTRA1 is expressed both intra- and extracellularly and participates in various biological processes, such as cell apoptosis, oxidative stress response (35-37) and maintenance of the BBB (38). The pathological changes observed in patients with cerebral autosomal recessive arteriopathy with subcortical infarcts and leukoencephalopathy include fibrosis, thinning of the adventitia of cerebral arterioles, loss of smooth muscle cells and thickening of the intima (39). Loss of HTRA1 impairs the maturation of smooth muscle cells and affects the function of vascular smooth muscle (40). Based on the moderate expression of HTRA1 in endothelial cells, it was hypothesized that these cells serve a role in this process. HtrA1 could enhance endothelial cell function by regulating intracellular signaling pathways and promoting cell proliferation and survival (41). However, HTRA1 also inhibits the proliferation of esophageal squamous cell carcinoma, ovarian and endometrial cancer, melanoma, neuroblastoma, liver cancer, and thyroid cancer cells (42,43). Additionally, in polypoid choroidal vasculopathy, HTRA1 OE decreases the proliferation of chorioretinal and human umbilical vein endothelial cells (44). HTRA1 promotes skin cell viability and proliferation, further confirming that it serves diverse roles in different types of tissue (45). The BBB permeability is associated with CSVD. Vascular endothelial cells and their tight junctions are key elements of the BBB function and structure (46). Disruption of this barrier involves increased paracellular permeability of endothelial cells, primarily due to the degradation of junctional proteins, such as ZO1, occludin and CLDN (46). The decrease in tight junction proteins leads to increased gaps between endothelial cells, making it easier for macromolecules and harmful substances to penetrate the BBB, thereby increasing the risk of neurological damage (47). The present study found elevated expression of tight junction-associated proteins and decreased cell permeability following HtrA1 OE, which further supported the hypothesis that HtrA1 OE contributes to the maintenance of the endothelial barrier integrity, which is key for preventing an increase in vascular permeability and inflammatory response (48). HtrA1 knockdown disrupts the intercellular tight junctions, leading to a decrease in endothelial barrier function, which may increase vascular permeability and promote inflammatory responses (49). The present endothelial cell-specific *HtrA1* knockdown mouse model demonstrated normal expression of HtrA1 contributes to the stabilization of BBB structure and function. The present findings suggested that *HTRA1* mutations contributed to the development of CSVD by affecting endothelial cell functionality and modulating the BBB permeability. Impaired BBB function is hypothesized to be a common pathological alteration in both CADASIL and HTRA1-associated CSVD with heterozygous mutations (38).

HTRA1 promotes apoptosis in tumor cells (50,51) in a caspase-dependent or caspase-independent manner, associated with the activation of caspase3 and caspase7 (52). HTRA1 OE triggers retinal epithelial cell apoptosis in age-related macular degeneration (53), and promotes fibroblast survival with antiapoptotic effects in a porcine wound healing model (54). In summary, HtrA1 inhibited apoptosis *in vivo* and *in vitro*. However, the effects of HtrA1 are contradictory, depending on the specific cell type and environmental context.

NOX4 is a key oxidase that serves a role in the oxidative stress response of endothelial cells (55). High NOX4

expression causes endothelial cell dysfunction, which leads to various cardiovascular diseases (56-58). Therefore, HtrA1 may protect cerebrovascular endothelial cells by inhibiting NOX4 expression, thereby maintaining normal cell function. Moreover, the absence of HtrA1 may result in increased sensitivity of endothelial cells to oxidative stress, exacerbating cell damage and apoptosis (59,60). In summary, oxidative stress is associated with the tight junctions between endothelial cells. Elevated oxidative stress, characterized by increased catalase expression and NADPH oxidase activity, leads to overall barrier dysfunction. Oxidative stress increases the BBB permeability (61), whereas NOX4 knockdown restores the expression of tight junction proteins and preserves the integrity of the endothelial cell barrier (62). Here, increased oxidative stress from NOX4 decreased the expression of tight junction proteins and increased the permeability of bEnd.3 cells, whereas inhibition of NOX4 expression reversed this effect.

Oxidative stress is associated with endothelial cell apoptosis and NOX4-dependent accumulation of ROS is a notable cause of apoptosis in vascular endothelial cells (63). NOX4 induces apoptosis in brain endothelial cells during inflammation-induced oxidative stress (55,64). It also induces apoptosis in arterial smooth muscle (65) and human umbilical vein endothelial cells (66). NOX4 knockdown decreases the production of ROS, caspase3 activity and the expression of Bcl-2 family members (67). Here, HtrA1 knockdown increased the expression of NOX4 and the levels of ROS and MDA and decreased SOD activity in bEnd.3 cells. Here, HtrA1 knockdown increased apoptosis in bEnd.3 cells, pointing to an essential role of HtrA1 in preserving tight junctions and cell barrier function. These results demonstrated the pathogenic mechanism of CSVD associated with HTRA1 and provided a basis for further investigations.

In the present study, downregulated *HtrA1* expression in mouse cerebral vascular endothelial cells resulted in increased anxiety-like behaviors, as well as notable decreases in memory and spatial learning abilities. The present study showed that HtrA1 was essential for regulating behavior in mice, particularly via oxidative stress-related signaling pathways. NOX4 OE is associated with the development of depressive symptoms, whereas its inhibition may improve depressive symptoms by decreasing oxidative stress and inflammatory responses (68). In addition, the GLX351322 intervention significantly increased the anxiety-like behaviors in mice in the OFT, suggesting that it may act by modulating the neurotransmitter system (69). As GLX351322 improved cognitive function in mice, HtrA1 may influence behavior via the NOX4-mediated oxidative stress pathway. These findings not only enhance understanding of the role of HtrA1 in hereditary CSVD but also provide a theoretical foundation for developing future therapeutic strategies for this condition (68,70,71). Consequently, targeting the NOX4 pathway may offer a promising therapeutic strategy for counteracting the deleterious effects of *HTRA1* mutations in patients with CSVD, ultimately improving neurological outcomes.

The present study has several limitations. While the present findings implicated the NOX4-mediated oxidative stress pathway in HTRA1-associated CSVD, peripheral blood transcriptomics serves primarily as a screening tool and does not constitute a direct readout of cerebral endothelial events. The restricted sample size (two families) and mutation spectrum (protease domain variants p.P285L/p.R302Q) may limit generalizability. Expanding cohorts to include mutations across functional domains may strengthen genotype-phenotype associations. The AAV/B130-shHtrA1 model incompletely recapitulates the human heterozygous partial loss-of-function effects. The shRNA knockdown model primarily mimics a haploinsufficiency state. However, certain *HTRA1* mutations may exert dominant-negative effects or alter protease function in manners not captured by gene knockdown. In the future, the use of knock-in animal models harboring specific patient-derived mutations may elucidate these potential mutation-specific effects. While the present study focused on endothelial cells, future investigations examining other key components of the neurovascular unit, such as pericytes, astrocytes and microglia, may be essential to elucidate the pathophysiology of CSVD. Although the present study identified HtrA1-NOX4 interactions, the precise regulatory mechanism remains unknown and studies using coimmunoprecipitation and chromatin accessibility assays are required.

Heterozygous *HTRA1* mutations underlie CSVD pathogenesis and mediate their effects via NOX4-mediated oxidative stress, which disrupts endothelial homeostasis and BBB integrity. By demonstrating the efficacy of NOX4 inhibition using GLX351322 in rescuing cerebrovascular and cognitive deficit, the present study provided preclinical evidence in support of the HTRA1-NOX4 interaction as a potential intervention target.

Acknowledgements

Not applicable.

Funding

The present study was supported by Shanxi Basic Research Program (grant nos. 202303021221222, 202403021212232, 202403021221350 and 202503021211261).

Availability of data and materials

The data generated in the present study may be found in the Gene Expression Omnibus under accession number GSE324041 or at the following URL: ncbi.nlm.nih.gov/geo/query/acc.cgi?acc=GSE324041.

Authors' contributions

SS, SX and CL conceived and designed the study. SS, MS, WJ, WY and XL conducted the experiments. SS, WY, and JW analyzed data. SS and JW confirm the authenticity of all the raw data. SS drafted the manuscript. SX and CL revised the manuscript. All authors have read and approved the final manuscript.

Ethics approval and consent to participate

The present study was approved by the ethics committee of the First Hospital of Shanxi Medical University, Taiyuan, China

(approval No. KYLL-2024-161). All animal experiments were approved by the Animal Welfare and Ethics Committee of the First Hospital of Shanxi Medical University (approval no. DWYJ-2025-304, Taiyuan, China). All participants provided written informed consent.

Patient consent for publication

Not applicable.

Competing interests

The authors declare that they have no competing interests.

References

1. Dupré N, Drieu A and Joutel A: Pathophysiology of cerebral small vessel disease: A journey through recent discoveries. J Clin Invest 134: e172841, 2024.
2. Salvadori E, Brambilla M, Maestri G, Nicotra A, Cova I, Pomati S and Pantoni L: The clinical profile of cerebral small vessel disease: Toward an evidence-based identification of cognitive markers. Alzheimers Dement 19: 244-260, 2023.
3. Chojdak-Łukasiewicz J, Dziadkowiak E, Zimny A and Paradowski B: Cerebral small vessel disease: A review. Adv Clin Exp Med 30: 349-356, 2021.
4. Gao Y, Li D, Lin J, Thomas AM, Miao J, Chen D, Li S and Chu C: Cerebral small vessel disease: Pathological mechanisms and potential therapeutic targets. Front Aging Neurosci 14: 961661, 2022.
5. Clausen T, Kaiser M, Huber R and Ehrmann M: HTRA proteases: Regulated proteolysis in protein quality control. Nat Rev Mol Cell Biol 12: 152-162, 2011.
6. Krojer T, Garrido-Franco M, Huber R, Ehrmann M and Clausen T: Crystal structure of DegP (HtrA) reveals a new protease-chaperone machine. Nature 416: 455-459, 2002.
7. Tossetta G, Fantone S, Licini C, Marzioni D and Mattioli-Belmonte M: The multifaced role of HtrA1 in the development of joint and skeletal disorders. Bone 157: 116350, 2022.
8. An E, Sen S, Park SK, Gordish-Dressman H and Hathout Y: Identification of novel substrates for the serine protease HTRA1 in the human RPE secretome. Invest Ophthalmol Vis Sci 51: 3379-3386, 2010.
9. Tiaden AN, Breiden M, Mirsaidi A, Weber FA, Bahrenberg G, Glanz S, Cinelli P, Ehrmann M and Richards PJ: Human serine protease HTRA1 positively regulates osteogenesis of human bone marrow-derived mesenchymal stem cells and mineralization of differentiating bone-forming cells through the modulation of extracellular matrix protein. Stem Cells 30: 2271-2282, 2012.
10. Shiga A, Nozaki H, Yokoseki A, Nihonmatsu M, Kawata H, Kato T, Koyama A, Arima K, Ikeda M, Katada S, *et al*: Cerebral small-vessel disease protein HTRA1 controls the amount of TGF-β1 via cleavage of proTGF-β1. Hum Mol Genet 20: 1800-1810, 2011.
11. Beaufort N, Scharrer E, Kremmer E, Lux V, Ehrmann M, Huber R, Houlden H, Werring D, Haffner C and Dichgans M: Cerebral small vessel disease-related protease HtrA1 processes latent TGF-β binding protein 1 and facilitates TGF-β signaling. Proc Natl Acad Sci USA 111: 16496-16501, 2014.
12. Hara K, Shiga A, Fukutake T, Nozaki H, Miyashita A, Yokoseki A, Kawata H, Koyama A, Arima K, Takahashi T, *et al*: Association of HTRA1 mutations and familial ischemic cerebral small-vessel disease. N Engl J Med 360: 1729-1739, 2009.
13. De Luca A, De Falco M, Severino A, Campioni M, Santini D, Baldi F, Paggi MG and Baldi A: Distribution of the serine protease HtrA1 in normal human tissues. J Histochem Cytochem 51: 1279-1284, 2003.
14. Yao Y and Li N: Effect of HtrA1 polymorphism on sensitivity to chemotherapy in patients with colon cancer. Med Sci Monit 26: e921933, 2020.
15. Tiaden AN and Richards PJ: The emerging roles of HTRA1 in musculoskeletal disease. Am J Pathol 182: 1482-1488, 2013.
16. Uemura M, Nozaki H, Kato T, Koyama A, Sakai N, Ando S, Kanazawa M, Hishikawa N, Nishimoto Y, Polavarapu K, *et al*: HTRA1-related cerebral small vessel disease: A review of the literature. Front Neurol 11: 545, 2020.
17. Liu JY, Zhu YC, Zhou LX, Wei YP, Mao CH, Cui LY, Peng B and Yao M: HTRA1-related autosomal dominant cerebral small vessel disease. Chin Med J (Engl) 134: 178-184, 2020.
18. Verdura E, Hervé D, Scharrer E, Amador Mdel M, Guyant-Maréchal L, Philippi A, Corlobé A, Bergametti F, Gazal S, Prieto-Morin C, *et al*: Heterozygous HTRA1 mutations are associated with autosomal dominant cerebral small vessel disease. Brain 138: 2347-2358, 2015.
19. Xu SY, Li HJ, Li S, Ren QQ, Liang JL and Li CX: Heterozygous pathogenic and likely pathogenic symptomatic HTRA1 variant carriers in cerebral small vessel disease. Int J Gen Med 16: 1149-1162, 2023.
20. Qian E, Uemura M, Kobayashi H, Nakamura S, Ozawa F, Yoshimatsu S, Ishikawa M, Onodera O, Morimoto S and Okano H: A human induced pluripotent stem cell model from a patient with hereditary cerebral small vessel disease carrying a heterozygous R302Q mutation in HTRA1. Inflamm Regen 43: 23, 2023.
21. Nozaki H, Kato T, Nihonmatsu M, Saito Y, Mizuta I, Noda T, Koike R, Miyazaki K, Kaito M, Ito S, *et al*: Distinct molecular mechanisms of HTRA1 mutants in manifesting heterozygotes with CARASIL. Neurology 86: 1964-1974, 2016.
22. Zellner A, Scharrer E, Arzberger T, Oka C, Domenga-Denier V, Joutel A, Lichtenthaler SF, Müller SA, Dichgans M and Haffner C: CADASIL brain vessels show a HTRA1 loss-of-function profile. Acta Neuropathol 136: 111-125, 2018.
23. Fasano A, Formichi P, Taglia I, Bianchi S, Di Donato I, Battisti C, Federico A and Dotti MT: HTRA1 expression profile and activity on TGF-β signaling in HTRA1 mutation carriers. J Cell Physiol 235: 7120-7127, 2020.
24. Livak KJ and Schmittgen TD: Analysis of relative gene expression data using real-time quantitative PCR and the 2(-Delta Delta C(T)) method. Methods 25: 402-408, 2001.
25. Xu SY, Li L, Sun WX, Shen JY and Li CX: Case report: Hypnic headache responds to agomelatine-a potential prophylactic treatment option. Front Neurol 14: 1179391, 2023.
26. Shang T, Pinho M, Ray D and Khera A: Two unique mutations in HTRA1-related cerebral small vessel disease in north America and Africa and literature review. J Stroke Cerebrovasc Dis 30: 106029, 2021.
27. Coste T, Hervé D, Neau JP, Jouvent E, Ba F, Bergametti F, Lamy M, Cogez J, Derache N, Schneckenburger R, *et al*: Heterozygous HTRA1 nonsense or frameshift mutations are pathogenic. Brain 144: 2616-2624, 2021.
28. Poulsen ET, Nielsen NS, Scavenius C, Mogensen EH, Risør MW, Runager K, Lukassen MV, Rasmussen CB, Christiansen G, Richner M, *et al*: The serine protease HtrA1 cleaves misfolded transforming growth factor β-induced protein (TGFBIp) and induces amyloid formation. J Biol Chem 294: 11817-11828, 2019.
29. May A, Su F, Dinh B, Ehlen R, Tran C, Adivikolanu H and Shaw PX: Ongoing controversies and recent insights of the ARMS2-HTRA1 locus in age-related macular degeneration. Exp Eye Res 210: 108605, 2021.
30. Wang Y, Shi C, Li Y, Yu W, Wei S, Fan Y, Mao C, Yang Z, Yu L, Zhao Z, *et al*: Genetic study of cerebral small vessel disease in Chinese Han population. Front Neurol 13: 829438, 2022.
31. Kobayashi Y, Kondo Y, Tazawa KI, Yamamoto K, Yoshinaga T, Nakamura K and Sekijima Y: HTRA1-related cerebral small-vessel disease causes cerebral microbleeds on the brainstem surface. J Neurol Sci 466: 123229, 2024.
32. Li MT, Ke J, Guo SF, Wu Y, Bian YF, Shan LL, Liu QY, Huo YJ, Guo C, Liu MY, *et al*: The protective effect of quercetin on endothelial cells injured by hypoxia and reoxygenation. Front Pharmacol 12: 732874, 2021.
33. Jiang S, Ma X, Chen Y, Gu B, Sun N and Xiao H: Effects of ginkgo diterpene lactone on brain inflammation and oxidative stress in rats with cognitive impairment of cerebral small vessel disease. Am J Transl Res 13: 6382-6390, 2021.
34. Lu YW, Hao RJ, Wei YY and Yu GR: The protective effect of harpagoside on angiotensin II (Ang II)-induced blood-brain barrier leakage in vitro. Phytother Res 35: 6241-6254, 2021.
35. Spugnini EP, Cardillo I, Fanciulli M, Crispi S, Vincenzi B, Boccellino M, Quagliuolo L and Baldi A: Electroporation as a strategy to promote HtrA1 gene uptake and chemotherapy efficacy in a mouse model of mesothelioma. Front Biosci (Elite Ed) 5: 974-981, 2013.
36. Tossetta G, Fantone S, Giannubilo SR, Ciavattini A, Senzacqua M, Frontini A and Marzioni D: HTRA1 in placental cell models: A possible role in preeclampsia. Curr Issues Mol Biol 45: 3815-3828, 2023.

37. Clawson GA, Bui V, Xin P, Wang N and Pan W: Intracellular localization of the tumor suppressor HtrA1/Prss11 and its association with HPV16 E6 and E7 proteins. J Cell Biochem 105: 81-88, 2008.
38. Li Y, Ying Y, Yao T, Jia X, Liang H, Tang W, Jia X, Song H, Shao X, Wang DJJ, *et al*: Decreased water exchange rate across blood-brain barrier in hereditary cerebral small vessel disease. Brain 146: 3079-3087, 2023.
39. Fukutake T: Cerebral autosomal recessive arteriopathy with subcortical infarcts and leukoencephalopathy (CARASIL): From discovery to gene identification. J Stroke Cerebrovasc Dis 20: 85-93, 2011.
40. Ikawati M, Kawaichi M and Oka C: Loss of HtrA1 serine protease induces synthetic modulation of aortic vascular smooth muscle cells. PLoS One 13: e0196628, 2018.
41. Pan S, Liu M, Xu H, Chuan J and Yang Z: Lipopolysaccharide activating NF-kB signaling by regulates HTRA1 expression in human retinal pigment epithelial cells. Molecules 28: 2236, 2023.
42. Xia J, Wang F, Wang L and Fan Q: Elevated serine protease HtrA1 inhibits cell proliferation, reduces invasion, and induces apoptosis in esophageal squamous cell carcinoma by blocking the nuclear factor-κB signaling pathway. Tumour Biol 34: 317-328, 2013.
43. Li Y, Yuan J, Rothzerg E, Wu X, Xu H, Zhu S and Xu J: Molecular structure and the role of high-temperature requirement protein 1 in skeletal disorders and cancers. Cell Prolif 53: e12746, 2020.
44. Jiang J, Huang L, Yu W, Wu X, Zhou P and Li X: Overexpression of HTRA1 leads to down-regulation of fibronectin and functional changes in RF/6A cells and HUVECs. PLoS One 7: e46115, 2012.
45. Yamawaki S, Naitoh M, Kubota H, Aya R, Katayama Y, Ishiko T, Tamura T, Yoshikawa K, Enoshiri T, Ikeda M and Suzuki S: HtrA1 is specifically up-regulated in active keloid lesions and stimulates keloid development. Int J Mol Sci 19: 1275, 2018.
46. Ballabh P, Braun A and Nedergaard M: The blood-brain barrier: An overview: Structure, regulation, and clinical implications. Neurobiol Dis 16: 1-13, 2004.
47. Song D, Lee JY, Park EC, Choi NE, Nam HY, Seo J and Lee J: Structure-activity relationship analysis of activity-based probes targeting HTRA family of serine proteases. Bioorg Med Chem Lett 87: 129259, 2023.
48. Yamamoto Y, Kojima K, Taura D, Sone M, Washida K, Egawa N, Kondo T, Minakawa EN, Tsukita K, Enami T, *et al*: Human iPS cell-derived mural cells as an in vitro model of hereditary cerebral small vessel disease. Mol Brain 13: 38, 2020.
49. Guo F, Tao X, Wu Y, Dong D, Zhu Y, Shang D and Xiang H: Carfilzomib relieves pancreatitis-initiated pancreatic ductal adenocarcinoma by inhibiting high-temperature requirement protein A1. Cell Death Discov 10: 58, 2024.
50. Chien J, Staub J, Hu SI, Erickson-Johnson MR, Couch FJ, Smith DI, Crowl RM, Kaufmann SH and Shridhar V: A candidate tumor suppressor HtrA1 is downregulated in ovarian cancer. Oncogene 23: 1636-1644, 2004.
51. Yu T, Chen CZ and Xing YQ: Inhibition of cell proliferation, migration and apoptosis in blue-light illuminated human retinal pigment epithelium cells by down-regulation of HtrA1. Int J Ophthalmol 10: 524-529, 2017.
52. Chien J, Aletti G, Baldi A, Catalano V, Muretto P, Keeney GL, Kalli KR, Staub J, Ehrmann M, Cliby WA, *et al*: Serine protease HtrA1 modulates chemotherapy-induced cytotoxicity. J Clin Invest 116: 1994-2004, 2006.
53. Chen Y, Xing X, Dai W, Tian L, Dong Z and Yu S: Brain regions involved in fractional amplitude of low-frequency fluctuation in cluster headache patients: A resting-state functional MRI study. BMC Neurol 22: 336, 2022.
54. Sabino F, Madzharova E and Auf dem Keller U: Cell density-dependent proteolysis by HtrA1 induces translocation of zyxin to the nucleus and increased cell survival. Cell Death Dis 11: 674, 2020.
55. Basuroy S, Bhattacharya S, Leffler CW and Parfenova H: Nox4 NADPH oxidase mediates oxidative stress and apoptosis caused by TNF-alpha in cerebral vascular endothelial cells. Am J Physiol Cell Physiol 296: C422-C432, 2009.
56. Davis CM, Lyon-Scott K, Varlamov EV, Zhang WH and Alkayed NJ: Role of endothelial STAT3 in cerebrovascular function and protection from ischemic brain injury. Int J Mol Sci 23: 12167, 2022.
57. Kuppusamy M, Ottolini M and Sonkusare SK: Role of TRP ion channels in cerebral circulation and neurovascular communication. Neurosci Lett 765: 136258, 2021.
58. Alves JV, da Costa RM, Awata WMC, Bruder-Nascimento A, Singh S, Tostes RC and Bruder-Nascimento T: NADPH oxidase 4-derived hydrogen peroxide counterbalances testosterone-induced endothelial dysfunction and migration. Am J Physiol Endocrinol Metab 327: E1-E12, 2024.
59. Nivoit P, Mathivet T, Wu J, Salemkour Y, Sankar DS, Baudrie V, Bourreau J, Guihot AL, Vessieres E, Lemitre M, *et al*: Autophagy protein 5 controls flow-dependent endothelial functions. Cell Mol Life Sci 80: 210, 2023.
60. Storm J, Wu Y, Davies J, Moxon CA and Craig AG: Testing the effect of PAR1 inhibitors on Plasmodium falciparum-induced loss of endothelial cell barrier function. Wellcome Open Res 5: 34, 2020.
61. Lochhead JJ, McCaffrey G, Quigley CE, Finch J, DeMarco KM, Nametz N and Davis TP: Oxidative stress increases blood-brain barrier permeability and induces alterations in occludin during hypoxia-reoxygenation. J Cereb Blood Flow Metab 30: 1625-1636, 2010.
62. Jiang J, Huang K, Xu S, Garcia JGN, Wang C and Cai H: Targeting NOX4 alleviates sepsis-induced acute lung injury via attenuation of redox-sensitive activation of CaMKII/ERK1/2/MLCK and endothelial cell barrier dysfunction. Redox Biol 36: 101638, 2020.
63. Ma Y, Li W, Yin Y and Li W: AST IV inhibits H_2O_2-induced human umbilical vein endothelial cell apoptosis by suppressing Nox4 expression through the TGF-β1/Smad2 pathway. Int J Mol Med 35: 1667-1674, 2015.
64. Liu J, Chandaka GK, Zhang R and Parfenova H: Acute antioxidant and cytoprotective effects of sulforaphane in brain endothelial cells and astrocytes during inflammation and excitotoxicity. Pharmacol Res Perspect 8: e00630, 2020.
65. Pedruzzi E, Guichard C, Ollivier V, Driss F, Fay M, Prunet C, Marie JC, Pouzet C, Samadi M, Elbim C, *et al*: NAD(P)H oxidase Nox-4 mediates 7-ketocholesterol-induced endoplasmic reticulum stress and apoptosis in human aortic smooth muscle cells. Mol Cell Biol 24: 10703-10717, 2004.
66. Simon F and Fernández R: Early lipopolysaccharide-induced reactive oxygen species production evokes necrotic cell death in human umbilical vein endothelial cells. J Hypertens 27: 1202-1216, 2009.
67. Zhang Q, Liu X, Li N, Zhang J, Yang J and Bu P: Sirtuin 3 deficiency aggravates contrast-induced acute kidney injury. J Transl Med 16: 313, 2018.
68. Liao J, Peng B, Huang G, Diao C, Qin Y, Hong Y, Lin J, Lin Y, Jiang L, Tang N, *et al*: Inhibition of NOX4 with GLX351322 alleviates acute ocular hypertension-induced retinal inflammation and injury by suppressing ROS mediated redox-sensitive factors activation. Biomed Pharmacother 165: 115052, 2023.
69. Tao W, Yu L, Shu S, Liu Y, Zhuang Z, Xu S, Bao X, Gu Y, Cai F, Song W, *et al*: miR-204-3p/Nox4 mediates memory deficits in a mouse model of Alzheimer's disease. Mol Ther 29: 396-408, 2021.
70. Chen M, Yang S, Wu Y, Zhao Z, Zhai X and Dong D: High temperature requirement A1 in cancer: Biomarker and therapeutic target. Cancer Cell Int 21: 513, 2021.
71. Anvari E, Wikström P, Walum E and Welsh N: The novel NADPH oxidase 4 inhibitor GLX351322 counteracts glucose intolerance in high-fat diet-treated C57BL/6 mice. Free Radic Res 49: 1308-1318, 2015.